

DiffusionShield: A Watermark for Data Copyright Protection against Generative Diffusion Models

Yingqian Cui^{*1} Jie Ren^{*1} Han Xu¹ Pengfei He¹ Hui Liu¹ Lichao Sun² Yue Xing³ Jiliang Tang¹

Abstract

Recently, Generative Diffusion Models (GDMs) have shown remarkable abilities in learning and generating images, fostering a large community of GDMs. However, the unrestricted proliferation has raised serious concerns on copyright issues. For example, artists become concerned that GDMs could effortlessly replicate their unique artworks without permission. In response to these challenges, we introduce a novel watermark scheme, DiffusionShield, against GDMs. It protects images from infringement by encoding the ownership message into an imperceptible watermark and injecting it into images. This watermark can be easily learned by GDMs and will be reproduced in generated images. By detecting the watermark in generated images, the infringement can be exposed with evidence. Benefiting from the uniformity of the watermarks and the joint optimization method, DiffusionShield ensures low distortion of the original image, high watermark detection performance, and lengthy encoded messages. We conduct rigorous and comprehensive experiments to show its effectiveness in defending against infringement by GDMs and its superiority over traditional watermark methods.

1. Introduction

Generative diffusion models (GDMs), such as Denoising Diffusion Probabilistic Models (DDPM) (Ho et al., 2020) have shown their great potential in generating high-quality images. This has also led to the growth of more advanced techniques, such as DALL·E2 (Ramesh et al., 2022), Stable Diffusion (Rombach et al., 2022), and ControlNet (Zhang &

^{*}Equal contribution ¹Department of Computer Science and Engineering, Michigan State University, US. ²Department of Computer Science and Engineering, Lehigh University ³Department of Statistics and Probability, Michigan State University, US. Correspondence to: Yingqian Cui <cuiyingq@msu.edu>, Jie Ren <renjie3@msu.edu>.

Agrawala, 2023). In general, a GDM learns the distribution of a set of collected images, and can generate images that follow the learned distribution. As these techniques become increasingly popular, concerns have arisen regarding the copyright protection of creative works shared on the Internet. For instance, a fashion company may invest significant resources in designing a new fashion. After the company posts the pictures of this fashion to the public for browsing, an unauthorized entity can train their GDMs to mimic its style and appearance, generating similar images and producing products. This infringement highlights the pressing need for copyright protection mechanisms.

To provide protection for creative works, watermark techniques such as Cox et al. (2002); Podilchuk & Delp (2001); Zhu et al. (2018); Navas et al. (2008); Yu et al. (2021) are often applied, which aim to inject (invisible) watermarks into images and then detect them to track the malicious copy and accuse the infringement. However, directly applying these existing methods to GDMs still faces tremendous challenges. Indeed, since existing watermark methods have not specifically been designed for GDMs, they might be hard to learn by GDMs and could disappear in the generated images. Then the infringement may not be effectively verified and accused.

An empirical evidence can be found in Figure 1. We train two popular GDMs on a CIFAR10 dataset whose samples are watermarked by two representative watermark methods (Navas et al., 2008; Zhu et al., 2018), and we try to detect the watermarks in the GDM-generated images. The result demonstrates that the watermarks from these methods are either hardly learned and reproduced by GDM (e.g., FRQ (Navas et al., 2008)), or require a very large budget (the extent of image distortion) to partially maintain the watermarks (e.g., HiDDeN (Zhu et al., 2018)). Therefore, dedicated efforts are still greatly desired to devel-

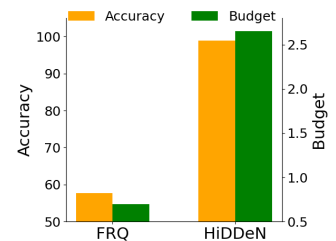


Figure 1. Watermark detection accuracy (%) on GDM-generated images and the corresponding budget (l_2 norm) of watermarks.

oping the watermark technique tailored for GDMs.

In this work, we argue that one critical factor that causes the inefficacy of these existing watermark techniques is the inconsistency of watermark patterns on different data samples. In methods such as Navas et al. (2008); Zhu et al. (2018), the watermark in each image from one owner is distinct. Thus, GDMs can hardly learn the distribution of watermarks and reproduce them in the generated samples. To address this challenge, we propose **DiffusionShield** which aims to enhance the “*pattern uniformity*” (Section 3.2) of the watermarks to make them consistent across different images. We first empirically show that watermarks with pattern uniformity are easy to be reproduced by GDMs in Section 3.2. Then, we provide corresponding theoretic analysis in two examples to demonstrate that the watermarks with pattern uniformity will be learned prior to other features in Section 3.5. The theoretical evidence further suggests that if unauthorized GDMs attempt to learn from the watermarked images, they are likely to learn the watermarks before the original data distribution.

Leveraging pattern uniformity, DiffusionShield designs a blockwise strategy to divide the watermarks into a sequence of basic patches, and a user has a specific sequence of basic patches which forms a watermark applied on all his/her images and encodes the copyright message. The watermark will repeatedly appear in the training set of GDMs, and thus makes it reproducible and detectable. In the case of multiple users, each user will have his/her own watermark pattern based on the encoded message. Furthermore, DiffusionShield introduces a joint optimization method for basic patches and watermark detectors to enhance each other, which achieves a smaller budget and higher accuracy. In addition, once the watermarks are obtained, DiffusionShield does not require re-training when there is an influx of new users and images, indicating the flexibility of DiffusionShield to accommodate multiple users. In summary, with the enhanced pattern uniformity in blockwise strategy and joint optimization, we can successfully secure the data copyright against infringement by GDMs.

2. Related Work

2.1. Generative Diffusion Models

In recent years, GDMs have made significant strides. A breakthrough in GDMs is achieved by DDPM (Nichol & Dhariwal, 2021), which demonstrates great superiority in generating high-quality images. The work of Ho & Salimans (2022) further advances the field by eliminating the need for classifiers in the training process. Song et al. (2020) presents Denoising Diffusion Implicit Models (DDIMs), a variant of GDMs with improved efficiency in sampling. Besides, techniques such as Rombach et al. (2022) achieve

high-resolution image synthesis and text-to-image synthesis. These advancements underscore the growing popularity and efficacy of GDM-based techniques.

To train GDMs, many existing methods rely on collecting a significant amount of training data from public resources (Deng et al., 2009; Yu et al., 2015; Guo et al., 2016). However, there is a concern that if a GDM is trained on copyrighted material and produces outputs similar to the original copyrighted works, it could potentially infringe on the copyright owner’s rights. This issue has already garnered public attention (Vincent, 2023), and our paper focuses on mitigating this risk by employing a watermarking technique to detect copyright infringements.

2.2. Image Watermarking

Image watermarking involves embedding invisible information into the carrier images and is commonly used to identify ownership of the copyright. Traditional watermarking techniques include spatial domain methods and frequency domain methods (Cox et al., 2002; Navas et al., 2008; Shih & Wu, 2003; Kumar, 2020). These techniques embed watermark information by modifying the pixel values (Cox et al., 2002), frequency coefficients (Navas et al., 2008), or both (Shih & Wu, 2003; Kumar, 2020). Recently, various digital watermarking approaches based on Deep Neural Networks (DNNs) have been proposed. For example, Zhu et al. (2018) uses an autoencoder-based network architecture, while Zhang et al. (2019) designs a GAN for watermark. Those techniques are then generalized to photographs (Tancik et al., 2020) and videos (Weng et al., 2019).

Notably, there are existing studies focusing on watermarking generative neural networks, such as GANs (Goodfellow et al., 2020) and image processing networks (Sehwag et al., 2022). Their goal is to safeguard the *intellectual property (IP) of generative models and generated images*, while our method is specifically designed for safeguarding *the copyright of data against potential infringement by these GDMs*. To accomplish their goals, the works Wu et al. (2020); Yu et al. (2021); Zhao et al. (2023b); Zhang et al. (2020b) embed imperceptible watermarks into every output of a generative model, enabling the defender to determine whether an image was generated by a specific model or not. Various approaches have been employed to inject watermarks, including reformulating the training objectives of the generative models (Wu et al., 2020), modifying the model’s training data (Yu et al., 2021; Zhao et al., 2023b), or directly conducting watermark embedding to the output images before they are presented to end-users (Zhang et al., 2020b).

3. Method

In this section, we first formally define the problem and the key notations. Next, we show that the “*pattern uniformity*” is a key factor for the watermark of generated samples.

Based on this, we introduce two essential components of our method, DiffusionShield, i.e., (i) blockwise watermark with pattern uniformity and (ii) joint optimization, and then provide theoretic analysis of pattern uniformity.

3.1. Problem Statement

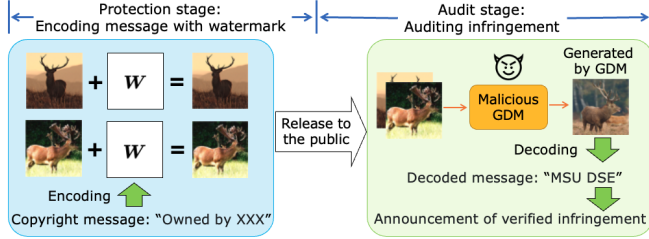


Figure 2. An overview of watermarking with two stages.

In this work, we consider two roles: (1) **a data owner** who holds the copyright of the data, releases the data solely for public browsing, and aspires to protect them from being replicated by GDMs, and (2) **a data offender** who employs a GDM on the released data to learn the creative works and infringe the copyright. Besides, since data are often collected from multiple sources to train GDMs in reality, we also consider a scenario where multiple owners protect their copyright against GDMs by encoding their own copyright information into watermarks. We first define the one-owner case, and then extend to the multiple-owner case:

• **Protection for one-owner case.** An image owner aims to release n images, $\{\mathbf{X}_{1:n}\}$, strictly for browsing. Each image \mathbf{X}_i has a shape of (U, V) where U and V are the height and width, respectively. As shown in Figure 2, the protection process generally comprises two stages: 1) *a protection stage* when the owner encodes the copyright information into the invisible watermark and adds it to the protected data; and 2) *an audit stage* when the owner examines whether a generated sample infringes upon their data. In the following, we introduce crucial definitions and notations.

- 1) *The protection stage* happens before the owner releases $\{\mathbf{X}_{1:n}\}$ to the public. To protect the copyright, the owner encodes the copyright message M into each of the invisible watermarks $\{\mathbf{W}_{1:n}\}$, and adds \mathbf{W}_i into \mathbf{X}_i to get a protected data $\tilde{\mathbf{X}}_i = \mathbf{X}_i + \mathbf{W}_i$. M contains information like texts that can signify the owners’ unique copyright. The images $\tilde{\mathbf{X}}_i$ and \mathbf{X} appear similar in human eyes with a small watermark budget $\|\mathbf{W}_i\|_p \leq \epsilon$. Instead of releasing $\{\mathbf{X}_{1:n}\}$, the owner releases the protected $\{\tilde{\mathbf{X}}_{1:n}\}$ for public browsing.
- 2) *The audit stage* refers to that the owner finds suspicious images which potentially offend the copyright of their images, and they scrutinize whether these images are generated from their released data. We assume that the data offender collects a dataset $\{\mathbf{X}_{1:N}^G\}$ that contains the protected images $\{\tilde{\mathbf{X}}_{1:n}\}$, i.e. $\{\tilde{\mathbf{X}}_{1:n}\} \subset \{\mathbf{X}_{1:N}^G\}$

where N is the total number of both protected and unprotected images ($N > n$). The data offender then trains a GDM, \mathcal{G} , from scratch to generate images, \mathbf{X}_G . If \mathbf{X}_G contains the copyright information of the data owner, once \mathbf{X}_G is inputted to a decoder \mathcal{D} , the copyright message should be decoded by \mathcal{D} .

• **Protection for multiple-owner case.** When there are K data owners to protect their distinct sets of images, we denote their sets of images as $\{\mathbf{X}_{1:n}^k\}$ where $k = 1, \dots, K$. Following the methodology of one-owner case, each owner can re-use the same encoding process and decoder to encode and decode distinct messages in different watermarks, \mathbf{W}_i^k , which signifies their specific copyright messages M^k . The protected version of images is denoted by $\tilde{\mathbf{X}}_i^k = \mathbf{X}_i^k + \mathbf{W}_i^k$. Then the protected images, $\{\tilde{\mathbf{X}}_{1:n}^k\}$, can be released by their respective owners for public browsing, ensuring their copyright is maintained. More details about the two protection cases can be found in Appendix A.

3.2. Pattern Uniformity

In this subsection, we uncover one important factor “*pattern uniformity*” which could be an important reason for the failure of existing watermark techniques. Previous studies (Sehwag et al., 2022; Um & Ye, 2023; Daras et al., 2023) observe that GDMs tend to learn data samples from high probability density regions in the data space and ignore the low probability density regions. However, many existing watermarks such as FRQ (Navas et al., 2008) and HiDDeN (Zhu et al., 2018) can only generate distinct watermarks for different data samples. Since their generated watermarks are dispersed, these watermarks cannot be effectively extracted and learned.

Observing the above, we formally define the “*pattern uniformity*” as the consistency of different watermarks injected for different samples:

$$Z = 1 - \frac{1}{n} \sum_{i=1}^n \left\| \frac{\mathbf{W}_i}{\|\mathbf{W}_i\|_2} - \mathbf{W}_{mean} \right\|_2, \quad (1)$$

$$\text{where } \mathbf{W}_{mean} = \frac{1}{n} \sum_{i=1}^n \frac{\mathbf{W}_i}{\|\mathbf{W}_i\|_2}.$$

The notation Z corresponds to the standard deviation of normalized watermarks.

We further conduct experiments to illustrate the importance of this “*pattern uniformity*”. In the experiment shown in Figure 3, we test the ability of DDPM in learning watermarks with different pattern uniformity.

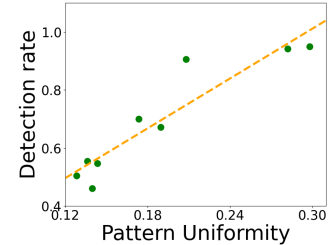


Figure 3. Uniformity vs. watermark detection rate.

The watermarks \mathbf{W}_i are random pictures whose pixel value is re-scaled by the budget σ , and the watermarked images are $\tilde{\mathbf{X}}_i = \mathbf{X}_i + \sigma \times \mathbf{W}_i$. More details about the settings for this watermark and the detector can be found in Appendix C.1.

Figure 3 illustrates a positive correlation between watermark detection rate in the GDM-generated images and pattern uniformity, which implies that pattern uniformity improves watermark reproduction. Based on pattern uniformity, in Section 3.3 and 3.4, we introduce how to design DiffusionShield, and in Section 3.5, we provide a theoretic analysis of the pattern uniformity based on two examples to justify that the watermarks will be first learned prior to other sparse hidden features and, thus, provide an effective protection.

3.3. Watermarks and Decoding Watermarks

In this subsection, we introduce our proposed approach, referred as DiffusionShield. This model is designed to resolve the problem of inadequate reproduction of prior watermarking approaches in generated images. It adopts a blockwise watermarking approach to augment pattern uniformity, which improves the reproduction of watermarks in generated images and enhances flexibility.

Blockwise watermarks. In DiffusionShield, to strengthen the pattern uniformity in $\{\mathbf{W}_{1:n}\}$, we use the same watermark \mathbf{W} for each \mathbf{X}_i from the same owner. The sequence of *basic patches* encodes the textual copyright message M of the owner. In detail, M is first converted into a sequence of binary numbers by predefined rules such as ASCII. To condense the sequence’s length, we convert the binary sequence into a B -nary sequence, denoted as $\{\mathbf{b}_{1:m}\}$, where m is the message length and B -nary denotes different numeral systems like quaternary ($B = 4$) and octal ($B = 8$). Accordingly, DiffusionShield partitions the whole watermark \mathbf{W} into a sequence of m patches, $\{\mathbf{w}_{1:m}\}$, to represent $\{\mathbf{b}_{1:m}\}$. Each patch is chosen from a candidate set of basic patch $\{\mathbf{w}^{(1:B)}\}$. The set $\{\mathbf{w}^{(1:B)}\}$ has B basic patch candidates with a shape (u, v) , which represent different values of the B -nary bits. The sequence of $\{\mathbf{w}_{1:m}\}$ denotes the B -nary bits $\{\mathbf{b}_{1:m}\}$ derived from M .

For example, in Figure 4, we have 4 patches ($B = 4$), and each of the patches has a unique pattern which represents 0, 1, 2, and 3. To encode the copyright message $M = \text{“Owned by XXX”}$, we first convert it into binary se-

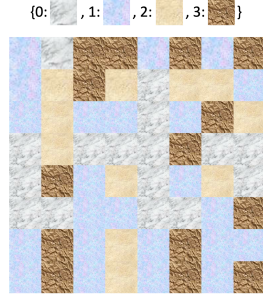


Figure 4. An 8×8 sequence of basic patches encoded with message “103313131232...”. Different patterns represent different basic patches.

quence “01001111 01110111...” based on ASCII, and transfer it into quaternary sequence $\{\mathbf{b}_{1:m}\}$, “103313131232...”. (The sequence length m should be less or equal to 8×8 , since there are only 8×8 patches in Figure 4.) Then we concatenate these basic patches in the order of $\{\mathbf{b}_{1:m}\}$ for the complete watermark \mathbf{W} and add \mathbf{W} to each image from the data owner. Once the offender uses GDMs to learn from it, the watermarks will appear in generated images, serving as an evidence of infringement.

Decoding the watermarks. DiffusionShield employs a decoder \mathcal{D}_θ by classification in patches, where θ is the parameters. \mathcal{D}_θ can classify \mathbf{w}_i into a bit \mathbf{b}_i . The decoder \mathcal{D}_θ accepts a watermarked image block, $\mathbf{x}_i + \mathbf{w}_i$, as input and outputs the bit value of \mathbf{w}_i , i.e., $\mathbf{b}_i = \mathcal{D}_\theta(\mathbf{x}_i + \mathbf{w}_i)$. The suspect generated image is partitioned into a sequence $\{(\mathbf{x} + \mathbf{w})_{1:m}\}$, and then is classified into $\{\mathbf{b}_{1:m}\} = \{\mathcal{D}_\theta(\mathbf{x}_i + \mathbf{w}_i) | i = 1, \dots, m\}$ in a patch-by-patch manner. If $\{\mathbf{b}_{1:m}\}$ is the B -nary message that we embed into the watermark, we can accurately identify the owner of the data, and reveal the infringement.

Remarks. Since we assign the same watermark \mathbf{W} to each image of one user, the designed watermark evidently has higher uniformity. Besides, DiffusionShield shows remarkable flexibility when applied to multiple-owner scenarios as basic patches and decoder can be reused by new owners.

3.4. Jointly Optimize Watermark and Decoder

While pattern uniformity facilitates the reproduction of watermarks in GDM-generated images, it does not guarantee the detection performance of the decoder \mathcal{D}_θ . Therefore, we further propose a joint optimization method to search for the optimal basic patch patterns and obtain the optimized detection decoder simultaneously. Ideally, the basic patches and the decoder should satisfy:

$$\mathbf{b}^{(i)} = \mathcal{D}_\theta(\mathbf{p} + \mathbf{w}^{(i)}) \text{ for } \forall i \in \{1, 2, \dots, B\}, \quad (2)$$

where $\mathbf{w}^{(i)}$ is one of the B basic patch candidates, $\mathbf{b}^{(i)}$ is the correct label for $\mathbf{w}^{(i)}$, and \mathbf{p} can be a random block with the same shape as $\mathbf{w}^{(i)}$ cropped from any image. The ideal decoder, capable of accurately predicting all the watermarked blocks, ensures that all embedded information can be decoded from the watermark. To increase the detection performance, we simultaneously optimize the basic patches and the decoder using the following bi-level objective:

$$\min_{\mathbf{w}^{1:B}} \min_{\theta} \mathbb{E} \left[\sum_{i=1}^B L_{\text{CE}} \left(\mathcal{D}_\theta \left(\mathbf{p} + \mathbf{w}^{(i)} \right), \mathbf{b}^{(i)} \right) \right] \text{ s.t. } \|\mathbf{w}^{(i)}\|_\infty \leq \epsilon,$$

where L_{CE} is the cross-entropy loss for the classification. The l_∞ budget is constrained by ϵ . To reduce the number of categories of basic patches, we set $\mathbf{w}^{(1)} = \mathbf{0}$, which means that the blocks without watermark should be classified as $\mathbf{b} = 1$. Thus, the bi-level optimization can be rewritten as:

$$\begin{cases} \theta^* = \arg \min_{\theta} \mathbb{E} \left[\sum_{i=1}^B L_{CE} \left(\mathcal{D}_{\theta} \left(\mathbf{p} + \mathbf{w}^{(i)} \right), \mathbf{b}^{(i)} \right) \right] \\ \mathbf{w}^{(2:B),*} = \arg \min_{\mathbf{w}^{(2:B)}} \mathbb{E} \left[\sum_{i=2}^B L_{CE} \left(\mathcal{D}_{\theta^*} \left(\mathbf{p} + \mathbf{w}^{(i)} \right), \mathbf{b}^{(i)} \right) \right] \\ \text{s.t. } \|\mathbf{w}^{(i)}\|_{\infty} \leq \epsilon. \end{cases} \quad (3)$$

The upper-level objective aims to increase the performance of \mathcal{D}_{θ} , while the lower-level objective optimizes the basic patches to facilitate their detection by the decoder. By the two levels of objectives, the basic patches and decoder potentially promote each other to achieve higher accuracy on a smaller budget. To ensure basic patches can be adapted to various image blocks and increase their flexibility, we use randomly cropped image blocks as the host images in the training process of basic patches and decoders. More details about the algorithm can be found in Appendix D.

3.5. Theoretic Analysis of Pattern Uniformity

In this subsection, we provide theoretic analysis with two examples, a linear regression model for supervised task, and a multilayer perceptron (MLP) with a general loss function (which can be a **generation** task), to justify that watermarks with pattern uniformity are stronger than other features, and machine learning models can learn features from watermarks earlier and more easily regardless of the type of tasks. Following the same idea, DiffusionShield provides an effective protection since GDMs have to learn watermarks first if they want to learn from protected images.

For both two examples, we use the same assumption for the features in the watermarked dataset. For simplicity, we assume the identical watermark is added onto each sample in the dataset. We impose the following data assumption, which is extended from the existing sparse coding model (Olshausen & Field, 1997; Mairal et al., 2010; Arora et al., 2016; Allen-Zhu & Li, 2022).

Assumption 3.1 (Sparse coding model with watermark). The observed data is $\mathbf{Z} = \mathbf{M}\mathbf{S}$, where $\mathbf{M} \in \mathbb{R}^{d \times d}$ is a unitary matrix, and $\mathbf{S} = (s_1, s_2, \dots, s_d)^{\top} \in \mathbb{R}^d$ is the hidden feature composed of d sparse features:

$$P(s_i \neq 0) = p, \text{ and } s_i^2 = \mathcal{O}(1/pd) \text{ when } s_i \neq 0. \quad (4)$$

$\|\cdot\|$ is L_2 norm. For $\forall i \in [d]$, $\mathbb{E}[s_i] = 0$. The watermarked data is $\tilde{\mathbf{Z}} = \mathbf{M}\mathbf{S} + \boldsymbol{\delta}$, and $\boldsymbol{\delta}$ is a constant watermark vector for all the data samples because of pattern uniformity.

For the linear regression task, $\mathbf{Y} = \mathbf{S}^{\top} \boldsymbol{\beta} + \boldsymbol{\epsilon}$ is the ground truth label, where $\boldsymbol{\epsilon} \sim \mathcal{N}(0, \sigma^2)$ is the noise and $\beta_i = \Theta(1)$ so that $Y^2 = \mathcal{O}_p(1)$. We represent the linear regression model as $\hat{\mathbf{Y}} = \tilde{\mathbf{Z}}^{\top} \mathbf{w}$, using the watermark data $\tilde{\mathbf{Z}}$, where $\mathbf{w} \in \mathbb{R}^{1 \times d}$ is the parameter to learn. The mean square error (MSE) loss for linear regression task can be represented as

$$L(\mathbf{w}) = (\tilde{\mathbf{Z}}^{\top} \mathbf{w} - \mathbf{S}^{\top} \boldsymbol{\beta} - \boldsymbol{\epsilon})^2.$$

Given the above problem setup, we have following result: Consider the initial stage of the training, i.e., \mathbf{w} is initialized

with $w_i \stackrel{\text{i.i.d.}}{\sim} \mathcal{N}(0, 1)$. With Assumption 3.1, the gradient, with respect to \mathbf{w} , of MSE loss for the linear regression model given infinite samples can be derived as

$$\mathbb{E} \left[\frac{\partial L}{\partial \mathbf{w}} \right] = \mathbb{E}[A(\mathbf{S})] + \mathbb{E}[B(\boldsymbol{\delta})], \quad (5)$$

where $\mathbb{E}[A(\mathbf{S})]$ is the hidden feature term that contains the gradient terms from hidden features, and $\mathbb{E}[B(\boldsymbol{\delta})]$ is the watermark term that contains the gradient terms from the watermark.

There are three observations. First, watermark is learned prior to other hidden features after initialization. If $\|\boldsymbol{\delta}\| \gg 1/\sqrt{d}$, then with high probability w.r.t. the initialization, $\mathbb{E}\|B(\boldsymbol{\delta})\| \gg \mathbb{E}\|A(\mathbf{S})\|$, and $\mathbb{E}\|B(\boldsymbol{\delta})\|$ is maximized with the best uniformity. Second, since $\|\boldsymbol{\delta}\| \ll 1/\sqrt{pd}$, the watermark $\boldsymbol{\delta}$ will be much smaller than any active hidden feature. Finally, when the training converges, the final trained model does not forget $\boldsymbol{\delta}$. (The proof is in Appendix B.1.)

In addition to the linear regression task, we extend our analysis to neural networks with a general loss to further explain the feasibility of the intuition for a generative task. We follow Assumption 3.1 and give the toy example for neural networks: We use an MLP with $\tilde{\mathbf{Z}}$ as input to fit a general loss $L(\mathcal{W}, \tilde{\mathbf{Z}})$. The loss $L(\mathcal{W}, \tilde{\mathbf{Z}})$ can be a classification or generation task. The notation \mathcal{W} is the parameter of it, and \mathcal{W}_1 is the first layer of \mathcal{W} . Under mild assumptions, we can derive the gradient with respect to each neuron in \mathcal{W}_1 into hidden feature term and watermark term as Eq. 5. When $1/\sqrt{d} \ll \|\boldsymbol{\delta}\| \ll 1/\sqrt{pd}$, the watermark term will have more influence and be learned prior to other hidden features in the first layer even though the watermark has a much smaller norm than each active hidden feature. (The proof can be found in Appendix B.2.)

With the theoretical analysis in the above two examples, we justify that the watermark with high pattern uniformity is easier/earlier to be learned than other sparse hidden features. It suggests if the authorized people use GDM to learn from the protected images, the GDM will first learn the watermarks before the data distribution. Therefore, our method can provide an effective protection against GDM. We also provide empirical evidence to support this analysis in Appendix B.3.

4. Experiment

In this section, we assess the efficacy of DiffusionShield across various budgets, datasets, and protection scenarios. We first introduce our experimental setups in Section 4.1. In Section 4.2, we evaluate the performance in terms of its accuracy and invisibility. Then we investigate the flexibility and efficacy in multiple-user cases, capacity for message length and robustness, from Section 4.3 to 4.6. We also evaluate the quality of generated images in Appendix H.

4.1. Experimental Settings

Datasets, baselines and GDM. We conduct the experiments using four datasets and compare DiffusionShield with four baseline methods. The datasets include CIFAR10 and CIFAR100, both with $(U, V) = (32, 32)$, STL10 with $(U, V) = (64, 64)$ and ImageNet-20 with $(U, V) = (256, 256)$. The baseline methods include Image Blending (IB) which is a simplified version of DiffusionShield without joint optimization, DWT-DCT-SVD based watermarking in the frequency domain (FRQ) (Navas et al., 2008), HiDDeN (Zhu et al., 2018), and DeepFake Fingerprint Detection (DFD) (Yu et al., 2021) (which is designed for DeepFake Detection and adapted to our data protection goal). In the audit stage, we use the improved DDPM (Nichol & Dhariwal, 2021) as the GDM to train on watermarked data. More details about baselines and improved DDPM is in Appendix C.4 and C.6, respectively.

Evaluation metrics. In our experiments, we generate T images from each GDM and decode copyright messages from them. We compare the effectiveness of watermarks in terms of their invisibility, the decoding performance, and the capacity to embed longer messages:

- **(Perturbation) Budget.** We use the LPIPS (Zhang et al., 2018) metric together with l_2 and l_∞ differences to measure the visual discrepancies between the original and watermarked images. The lower values of these metrics indicate better invisibility.
- **(Detection) Accuracy.** Following Yu et al. (2021) and Zhao et al. (2023c), we apply bit accuracy to evaluate the correctness of detected messages encoded. To compute bit accuracy, we transform the ground truth B -nary message $\{b_{1:m}\}$ and the decoded $\{\hat{b}_{1:m}\}$ back into binary messages $\{b'_{1:m \log_2 B}\}$ and $\{\hat{b}'_{1:m \log_2 B}\}$. The bit accuracy for one watermark is

$$\text{Bit-Acc} \equiv \frac{1}{m \log_2 B} \sum_{k=1}^{m \log_2 B} \mathbb{1} \left(b'_{1:m \log_2 B} = \hat{b}'_{1:m \log_2 B} \right).$$

The worst bit accuracy is expected to be 50%, which is equivalent to random guessing.

- **Message length.** The length of the encoded message reflects the capacity of encoding. To ensure the accuracy of FRQ and HiDDeN, we use a 16-bit and a 32-bit message for CIFAR images and a 64-bit one for STL10. For others, we encode 128 bits into CIFAR, 512 bits into STL10 and 256 bits into ImageNet.

Implementation details. We set $(u, v) = (4, 4)$ as the shape of the basic patches and set $B = 4$ for quarternary messages. We use ResNet (He et al., 2016) as the decoder to classify different basic patches. For the joint optimization, we use 5-step PGD (Madry et al., 2017) with $l_\infty \leq \epsilon$ to update the basic patches and use SGD to optimize the decoder. As mentioned in Section 3.1, the data offender may collect and train the watermarked images and non-watermarked

images together to train GDMs. Hence, in all the datasets, we designate one random class of images as watermarked images, while treating other classes as unprotected images. To generate images of the protected class, we either 1) use a **class-conditional** GDM to generate images from the specified class, or 2) apply a classifier to filter images of the protected class from the **unconditional** GDM’s output. The bit accuracy on unconditionally generated images may be lower than that of the conditional generated images since object classifiers cannot achieve 100% accuracy. In the joint optimization, we use SGD with 0.01 learning rate and 5×10^{-4} weight decay to train the decoder and we use 5-step PGD with step size to be 1/10 of the L_∞ budget to train the basic patches. More details are presented in Appendix C.3.

4.2. Results on Protection Performance against GDM

In this subsection, we show that DiffusionShield provides protection with high bit accuracy and good invisibility in Table 1. We compare on two groups of images: (1) the originally released images with watermarks (**Released**) and (2) the generated images from class-conditional GDM or unconditional GDM trained on the watermarked data (**Cond.** and **Uncond.**). Based on Table 1, we can see:

First, DiffusionShield can protect the images with the highest bit accuracy and the lowest budget among all the methods. For example, on CIFAR10 and STL10, with all the budgets from 1/255 to 8/255, DiffusionShield achieves almost 100% bit accuracy on released images and conditionally generated images, which is better than all the baseline methods. Even constrained by the smallest budget with an l_∞ norm of 1/255, DiffusionShield still achieves a high successful reproduction rate. On CIFAR100 and ImageNet, DiffusionShield with an l_∞ budget of 4/255 achieves a higher bit accuracy in generated images with a much lower l_∞ difference and LPIPS than baseline methods. For baselines, FRQ cannot be reproduced by GDM, while HiDDeN and DFD require a much larger perturbation budget over DiffusionShield (Image examples are shown in Appendix E). The accuracy of IB is much worse than the DiffusionShield with 1/255 budget on CIFAR10 and STL10. To explain IB, without joint optimization, the decoder cannot perform well on released images and thus cannot guarantee its accuracy on generated images, indicating the importance of joint optimization. To further illustrate the invisibility of DiffusionShield, we demonstrate a visualization of its impact on the image feature space in Appendix J. It clearly shows that our method introduces negligible alterations to images’ features.

Second, enforcing pattern uniformity can promote the reproduction of watermarks in generated images. In Table 1, we can see that the bit accuracy of the conditionally generated images watermarked by DiffusionShield is as high as that of released images with a proper budget. In addition to DiffusionShield, IB’s accuracy in released data and conditionally generated data are also similar. This is because

Table 1. Bit accuracy (%) and budget of the watermark

| | | IB | FRQ | HiDDeN | DFD | DiffusionShield (ours) | | | | |
|-------------|--------------------|------------|---------|---------|----------------|------------------------|----------------|---------|-----------------|-----------------|
| CIFAR10 | Budget | l_∞ | 7/255 | 13/255 | 65/255 | 28/255 | 1/255 | 2/255 | 4/255 | 8/255 |
| | | l_2 | 0.52 | 0.70 | 2.65 | 1.21 | 0.18 | 0.36 | 0.72 | 1.43 |
| | | LPIPS | 0.01582 | 0.01790 | 0.14924 | 0.07095 | 0.00005 | 0.00020 | 0.00120 | 0.01470 |
| | Accuracy | Released | 87.2767 | 99.7875 | 99.0734 | 95.7763 | 99.6955 | 99.9466 | 99.9909 | 99.9933 |
| | | Cond. | 87.4840 | 57.7469 | 98.9250 | 93.5703 | 99.8992 | 99.9945 | 100.0000 | 99.9996 |
| | | Uncond. | 81.4839 | 55.6907 | 97.1536 | 89.1977 | 93.8186 | 95.0618 | 96.8904 | 96.0877 |
| | Pattern Uniformity | | 0.963 | 0.056 | 0.260 | 0.236 | 0.974 | 0.971 | 0.964 | 0.954 |
| CIFAR100 | Budget | l_∞ | 7/255 | 14/255 | 75/255 | 44/255 | 1/255 | 2/255 | 4/255 | 8/255 |
| | | l_2 | 0.52 | 0.69 | 3.80 | 1.58 | 0.18 | 0.36 | 0.72 | 1.43 |
| | | LPIPS | 0.00840 | 0.00641 | 0.16677 | 0.03563 | 0.00009 | 0.00013 | 0.00134 | 0.00672 |
| | Accuracy | Released | 84.6156 | 99.5250 | 99.7000 | 96.1297 | 99.5547 | 99.9297 | 99.9797 | 99.9922 |
| | | Cond. | 54.3406 | 54.4438 | 95.8640 | 90.5828 | 52.0078 | 64.3563 | 99.8000 | 99.9984 |
| | | Uncond. | 52.6963 | 54.6370 | 81.9852 | 79.0234 | 52.9576 | 53.1436 | 85.7057 | 91.2946 |
| | Pattern Uniformity | | 0.822 | 0.107 | 0.161 | 0.180 | 0.854 | 0.855 | 0.836 | 0.816 |
| STL10 | Budget | l_∞ | 8/255 | 14/255 | 119/255 | 36/255 | 1/255 | 2/255 | 4/255 | 8/255 |
| | | l_2 | 1.09 | 1.40 | 7.28 | 2.16 | 0.38 | 0.76 | 1.51 | 3.00 |
| | | LPIPS | 0.06947 | 0.02341 | 0.32995 | 0.09174 | 0.00026 | 0.00137 | 0.00817 | 0.03428 |
| | Accuracy | Released | 92.5895 | 99.5750 | 97.2769 | 94.2813 | 99.4969 | 99.9449 | 99.9762 | 99.9926 |
| | | Cond. | 96.0541 | 54.3945 | 96.5164 | 94.7236 | 95.4848 | 99.8164 | 99.8883 | 99.9828 |
| | | Uncond. | 89.2259 | 56.3038 | 91.3919 | 91.8919 | 82.5841 | 93.4693 | 96.1360 | 95.0586 |
| | Pattern Uniformity | | 0.895 | 0.071 | 0.155 | 0.203 | 0.924 | 0.921 | 0.915 | 0.907 |
| ImageNet-20 | Budget | l_∞ | - | 20/255 | 139/255 | 88/255 | 1/255 | 2/255 | 4/255 | 8/255 |
| | | l_2 | - | 5.60 | 25.65 | 21.68 | 1.17 | 2.33 | 4.64 | 9.12 |
| | | LPIPS | - | 0.08480 | 0.44775 | 0.30339 | 0.00019 | 0.00125 | 0.00661 | 0.17555 |
| | Accuracy | Released | - | 99.8960 | 98.0625 | 99.3554 | 99.9375 | 99.9970 | 99.9993 | 100.0000 |
| | | Cond. | - | 50.6090 | 98.2500 | 81.3232 | 53.6865 | 53.7597 | 99.9524 | 100.0000 |
| | Pattern Uniformity | | - | 0.061 | 0.033 | 0.041 | 0.941 | 0.930 | 0.908 | 0.885 |

IB is a simplified version of our method without joint optimization and also has high pattern uniformity. In contrast, other methods without pattern uniformity all suffer from a drop of accuracy from released images to conditionally generated images, especially FRQ, which has pattern uniformity lower than 0.11 and an accuracy level on par with a random guess. This implies that the decoded information in watermarks with high pattern uniformity (e.g., IB and ours in CIFAR10 are higher than 0.95) does not change much from released images to generated images and the watermarks can be exactly and easily captured by GDM. Notably, the performance drop on CIFAR100 and ImageNet in 1/255 and 2/255 is also partially due to the low watermark rate. In fact, both a small budget and a low watermark rate can hurt the reproduction of watermarks in generated images. In Appendix F, we discuss the effectiveness when watermark rate is low. We find that in multiple user case, even though the watermark rate for each user is low and they encode different messages and do not share the pattern uniformity, our method can still performs well.

In addition to the four baselines, we have also compared DiffusionShield with three other watermarking approaches, i.e., IGA (Zhang et al., 2020a), MBRS (Jia et al., 2021), and CIN (Ma et al., 2022). Overall, DiffusionShield still demonstrates a better trade-off between bit accuracy and budget compared to the other methods. The comparison

results can be found in Appendix C.5.

4.3. Flexibility and Efficacy in Multiple-user Case

In this subsection, we demonstrate that DiffusionShield is flexible to be transferred to new users while maintaining good protection against GDMs. We assume that multiple copyright owners are using DiffusionShield to protect their images, and different copyright messages should be encoded into the images from different copyright owners.

In Table 2, we use one class in the dataset as the first owner and the other classes as the new owners. The basic patches (with 4/255 l_∞ budget) and decoder are optimized on the first

Table 2. Average bit accuracy (%) across different numbers of copyright owners (on class-conditional GDM).

| owners | CIFAR-10 | CIFAR-100 |
|--------|----------|-----------|
| 1 | 100.0000 | 99.8000 |
| 4 | 99.9986 | 99.9898 |
| 10 | 99.9993 | 99.9986 |

class and re-used to protect the new classes. Images within the same class have the same message embedded, while images from different classes have distinct messages embedded in them. After reordering the basic patches for different messages, transferring from one class to the other classes does not take any additional calculation, and is efficient. We train class-conditional GDM on all of the protected data and get the average bit accuracy across classes. As shown in Table 2, on both CIFAR10 and CIFAR100, when we reorder

the basic patches to protect the other 3 classes or 9 classes, the protection performance is almost the same as the one class case, with bit accuracy all close to 100%. Besides flexibility, our watermarks can protect each of the multiple users and can distinguish them clearly even when their data are mixed by the data offender.

4.4. Generalization to Fine-tuning GDMs

In this subsection, we test the performance of our method when generalized to the fine-tuning GDMs (Rombach et al., 2022), which is also a common strategy for learning and generating images. Fine-tuning is a more difficult task compared to the training-from-scratch setting because fine-tuning only changes the GDM parameters to a limited extent. This change may be not sufficient to learn all the features in the fine-tuned dataset, therefore, the priority by pattern uniformity becomes even more important. To better generalize our method to the fine-tuning case, we enhance the uniformity in hidden space instead of pixel space, and limit l_2 norm instead of l_∞ norm. More details of fine-tuning and its experiment settings can be found in Appendix I. We assume that the data offender fine-tunes Stable Diffusion (Rombach et al., 2022) to learn the style of *pokemon-blip-captions* dataset (Pinkney, 2022). In Table 3, we compare the budget and bit accuracy of our method with three baselines. The observation is similar to that in Table 1. Although FRQ has a lower budget than ours, the bit accuracy on generated images is much worse. DFD has bit accuracy of 90.31%, but the budget is three times of ours. HiDDeN is worse than ours in both budget and bit accuracy. We further investigate the impact of the watermark on the hidden space in Appendix J, which aligns with the metrics presented in Table 3. In summary, our method has the highest accuracy in both released and generated data.

4.5. Capacity for Message Length

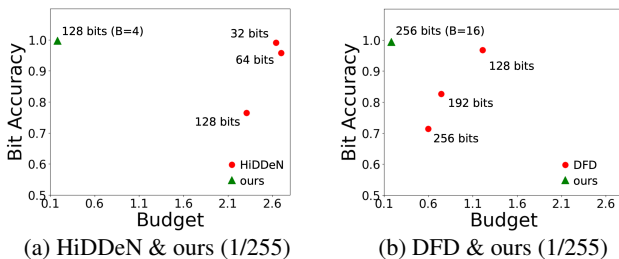


Figure 5. Bit acc. and l_2 of different message lengths

The capacity of embedding longer messages is important for watermarking methods since encoding more information can provide more conclusive evidence of infringement. In this subsection, we show the superiority of DiffusionShield over other methods in achieving high watermark capacity. Figure 5 shows the bit accuracy and l_2 budgets of water-

marks with different message lengths on the released protected images in CIFAR10. In Figure 5(a), we can see that HiDDeN consistently requires a large budget across varying message lengths, and its accuracy diminishes to 77% at 128 bits. Conversely, DiffusionShield maintains nearly 100% accuracy at 128 bits, even with a much smaller budget. Similarly, in Figure 5(b), ours maintains longer capacity with better accuracy and budget than DFD. This indicates that DiffusionShield has much greater capacity compared to HiDDeN and DFD and can maintain good performance even with increased message lengths.

4.6. Robustness of DiffusionShield

Robustness of watermarks is important since there is a risk that the watermarks may be distorted by disturbances, such as image corruption due to deliberate

| | DFD | HiDDeN | Ours |
|------------------|-------|--------|-------|
| No corrupt | 93.57 | 98.93 | 99.99 |
| Gaussian noise | 68.63 | 83.59 | 81.93 |
| Low-pass filter | 88.94 | 81.05 | 99.86 |
| Greyscale | 50.82 | 97.81 | 99.81 |
| JPEG comp. | 62.52 | 74.84 | 94.45 |
| Resize (Larger) | 93.20 | 79.69 | 99.99 |
| Resize (Smaller) | 92.38 | 83.13 | 99.30 |
| Wm. removal | 91.11 | 82.20 | 99.95 |

post-processing activities during the images' circulation, the application of speeding-up sampling methods in the GDM (Song et al., 2020), or different training hyper-parameters used to train GDM. This subsection demonstrates that DiffusionShield is robust in accuracy on generated images when corrupted. In Appendix G.2 and G.3, we show similar conclusions when sampling procedure is fastened and hyper-parameters are changed.

We consider Gaussian noise, low-pass filter, greyscale, JPEG compression, resizing, and the watermark removal attack proposed by Zhao et al. (2023a) to test the robustness of DiffusionShield against image corruptions. Details about the severity of the corruptions are shown in Appendix G.1. Different from the previous experiments, during the protection stage, we augment our method by incorporating corruptions into the joint optimization. Each corruption is employed after the basic patches are added to the images. Table 4 shows the bit accuracy of DiffusionShield (with $8/255 l_\infty$ budget) on corrupted generated images. It maintains accuracy above 99.8% under Greyscale, low-pass filter, resizing to larger size and watermark removal attack, nearly matching the accuracy achieved without corruption. In other corruptions, our method performs better than baselines except HiDDeN in Gaussian noise. In contrast, DFD has a significant reduce in Gaussian noise, Greyscale and JPEG compression, and HiDDeN shows a poor performance under low-pass filter and JPEG Compression. From these results, we can see that DiffusionShield is robust against image corruptions.

5. Conclusion

In this paper, we introduce DiffusionShield, a watermark to protect data copyright, which is motivated by our ob-

ervation that the pattern uniformity can effectively assist the watermark to be captured by GDMs. By enhancing the pattern uniformity of watermarks and leveraging a joint optimization method, DiffusionShield successfully secures copyright with better accuracy and a smaller budget. Theoretic analysis and experimental results demonstrate the superior performance of DiffusionShield.

6. Impact Statements

The development of DiffusionShield may have far-reaching implications across various domains.

1. **Art and creative industries.** The proposed watermarking scheme, DiffusionShield, holds immense potential for safeguarding the intellectual property of artists against unauthorized replication of their creative works by GDMs. It offers a much-needed solution to an emerging problem in the digital age, where the line between creativity and plagiarism can be blurred by advanced technology.
2. **Generative model and AI community.** This paper paves the way for responsible and ethical use of GDMs. It can encourage researchers, developers, and users of GDMs to respect the intellectual property rights of creators, fostering a more ethical landscape within the AI community.
3. **Legal frameworks and policies.** The implementation of DiffusionShield could impact copyright laws and policies. It provides a technical solution to expose copyright infringement with concrete evidence, contributing to more effective enforcement of digital copyright laws.
4. **Digital media and information.** By ensuring that the ownership information is encoded within an imperceptible watermark, this technology can help maintain the integrity of media and information. It reduces the risk of misattributed or misrepresented content, which is especially crucial in today’s digital age.

References

Allen-Zhu, Z. and Li, Y. Feature purification: How adversarial training performs robust deep learning. In *2021 IEEE 62nd Annual Symposium on Foundations of Computer Science (FOCS)*, pp. 977–988. IEEE, 2022.

Arora, S., Li, Y., Liang, Y., Ma, T., and Risteski, A. A latent variable model approach to pmi-based word embeddings. *Transactions of the Association for Computational Linguistics*, 4:385–399, 2016.

Ba, J., Erdogdu, M., Suzuki, T., Wu, D., and Zhang, T. Generalization of two-layer neural networks: An asymptotic viewpoint. In *International conference on learning representations*, 2019.

Chen, T., Kornblith, S., Norouzi, M., and Hinton, G. A simple framework for contrastive learning of visual representations. In *International conference on machine learning*, pp. 1597–1607. PMLR, 2020.

Cox, I., Miller, M., Bloom, J., and Honsinger, C. Digital watermarking. *Journal of Electronic Imaging*, 11(3):414–414, 2002.

Daras, G., Dagan, Y., Dimakis, A. G., and Daskalakis, C. Consistent diffusion models: Mitigating sampling drift by learning to be consistent. *arXiv preprint arXiv:2302.09057*, 2023.

Deng, J., Dong, W., Socher, R., Li, L.-J., Li, K., and Fei-Fei, L. Imagenet: A large-scale hierarchical image database. In *2009 IEEE conference on computer vision and pattern recognition*, pp. 248–255. Ieee, 2009.

Goodfellow, I., Pouget-Abadie, J., Mirza, M., Xu, B., Warde-Farley, D., Ozair, S., Courville, A., and Bengio, Y. Generative adversarial networks. *Communications of the ACM*, 63(11):139–144, 2020.

Guo, Y., Zhang, L., Hu, Y., He, X., and Gao, J. Ms-celeb-1m: A dataset and benchmark for large-scale face recognition. In *European conference on computer vision*, pp. 87–102. Springer, 2016.

He, K., Zhang, X., Ren, S., and Sun, J. Deep residual learning for image recognition. In *Proceedings of the IEEE conference on computer vision and pattern recognition*, pp. 770–778, 2016.

Ho, J. and Salimans, T. Classifier-free diffusion guidance. *arXiv preprint arXiv:2207.12598*, 2022.

Ho, J., Jain, A., and Abbeel, P. Denoising diffusion probabilistic models. *Advances in Neural Information Processing Systems*, 33:6840–6851, 2020.

Jia, Z., Fang, H., and Zhang, W. Mbrs: Enhancing robustness of dnn-based watermarking by mini-batch of real and simulated jpeg compression. In *Proceedings of the 29th ACM international conference on multimedia*, pp. 41–49, 2021.

Kumar, A. A review on implementation of digital image watermarking techniques using lsb and dwt. *Information and Communication Technology for Sustainable Development: Proceedings of ICT4SD 2018*, pp. 595–602, 2020.

- Ma, R., Guo, M., Hou, Y., Yang, F., Li, Y., Jia, H., and Xie, X. Towards blind watermarking: Combining invertible and non-invertible mechanisms. In *Proceedings of the 30th ACM International Conference on Multimedia*, pp. 1532–1542, 2022.
- Madry, A., Makelov, A., Schmidt, L., Tsipras, D., and Vladu, A. Towards deep learning models resistant to adversarial attacks. *arXiv preprint arXiv:1706.06083*, 2017.
- Mairal, J., Bach, F., Ponce, J., and Sapiro, G. Online learning for matrix factorization and sparse coding. *Journal of Machine Learning Research*, 11(1), 2010.
- Navas, K., Ajay, M. C., Lekshmi, M., Archana, T. S., and Sasikumar, M. Dwt-dct-svd based watermarking. In *2008 3rd International Conference on Communication Systems Software and Middleware and Workshops (COM-SWARE'08)*, pp. 271–274. IEEE, 2008.
- Nichol, A. Q. and Dhariwal, P. Improved denoising diffusion probabilistic models. In *International Conference on Machine Learning*, pp. 8162–8171. PMLR, 2021.
- Olshausen, B. A. and Field, D. J. Sparse coding with an overcomplete basis set: A strategy employed by v1? *Vision research*, 37(23):3311–3325, 1997.
- Pinkney, J. N. M. Pokemon blip captions. <https://huggingface.co/datasets/lambdalabs/pokemon-blip-captions/>, 2022.
- Podilchuk, C. I. and Delp, E. J. Digital watermarking: algorithms and applications. *IEEE signal processing Magazine*, 18(4):33–46, 2001.
- Ramesh, A., Dhariwal, P., Nichol, A., Chu, C., and Chen, M. Hierarchical text-conditional image generation with clip latents. *arXiv preprint arXiv:2204.06125*, 2022.
- Rombach, R., Blattmann, A., Lorenz, D., Esser, P., and Ommer, B. High-resolution image synthesis with latent diffusion models. In *Proceedings of the IEEE/CVF Conference on Computer Vision and Pattern Recognition*, pp. 10684–10695, 2022.
- Sehwag, V., Hazirbas, C., Gordo, A., Ozgenel, F., and Canton, C. Generating high fidelity data from low-density regions using diffusion models. In *Proceedings of the IEEE/CVF Conference on Computer Vision and Pattern Recognition*, pp. 11492–11501, 2022.
- Shih, F. Y. and Wu, S. Y. Combinational image watermarking in the spatial and frequency domains. *Pattern Recognition*, 36(4):969–975, 2003.
- Song, J., Meng, C., and Ermon, S. Denoising diffusion implicit models. *arXiv preprint arXiv:2010.02502*, 2020.
- Tancik, M., Mildenhall, B., and Ng, R. Stegastamp: Invisible hyperlinks in physical photographs. In *Proceedings of the IEEE/CVF conference on computer vision and pattern recognition*, pp. 2117–2126, 2020.
- Um, S. and Ye, J. C. Don't play favorites: Minority guidance for diffusion models. *arXiv preprint arXiv:2301.12334*, 2023.
- Vincent, J. Ai art copyright lawsuit: Getty images and stable diffusion. <https://www.theverge.com/2023/2/6/23587393>, Feb 2023. Accessed: May 12, 2023.
- von Platen, P., Patil, S., Lozhkov, A., Cuenca, P., Lambert, N., Rasul, K., Davaadorj, M., and Wolf, T. Diffusers: State-of-the-art diffusion models. <https://github.com/huggingface/diffusers>, 2022.
- Weng, X., Li, Y., Chi, L., and Mu, Y. High-capacity convolutional video steganography with temporal residual modeling. In *Proceedings of the 2019 on international conference on multimedia retrieval*, pp. 87–95, 2019.
- Wu, H., Liu, G., Yao, Y., and Zhang, X. Watermarking neural networks with watermarked images. *IEEE Transactions on Circuits and Systems for Video Technology*, 31(7):2591–2601, 2020.
- Yu, F., Seff, A., Zhang, Y., Song, S., Funkhouser, T., and Xiao, J. Lsun: Construction of a large-scale image dataset using deep learning with humans in the loop. *arXiv preprint arXiv:1506.03365*, 2015.
- Yu, N., Skripniuk, V., Abdelnabi, S., and Fritz, M. Artificial fingerprinting for generative models: Rooting deepfake attribution in training data. In *Proceedings of the IEEE/CVF International conference on computer vision*, pp. 14448–14457, 2021.
- Zhang, H., Wang, H., Cao, Y., Shen, C., and Li, Y. Robust data hiding using inverse gradient attention. *arXiv preprint arXiv:2011.10850*, 2020a.
- Zhang, J., Chen, D., Liao, J., Fang, H., Zhang, W., Zhou, W., Cui, H., and Yu, N. Model watermarking for image processing networks. In *Proceedings of the AAAI conference on artificial intelligence*, volume 34, pp. 12805–12812, 2020b.
- Zhang, L. and Agrawala, M. Adding conditional control to text-to-image diffusion models. *arXiv preprint arXiv:2302.05543*, 2023.
- Zhang, R., Isola, P., Efros, A. A., Shechtman, E., and Wang, O. The unreasonable effectiveness of deep features as a

perceptual metric. In *Proceedings of the IEEE conference on computer vision and pattern recognition*, pp. 586–595, 2018.

Zhang, R., Dong, S., and Liu, J. Invisible steganography via generative adversarial networks. *Multimedia tools and applications*, 78:8559–8575, 2019.

Zhao, X., Zhang, K., Wang, Y.-X., and Li, L. Generative autoencoders as watermark attackers: Analyses of vulnerabilities and threats. *arXiv preprint arXiv:2306.01953*, 2023a.

Zhao, Y., Liu, B., Ding, M., Liu, B., Zhu, T., and Yu, X. Proactive deepfake defence via identity watermarking. In *Proceedings of the IEEE/CVF Winter Conference on Applications of Computer Vision*, pp. 4602–4611, 2023b.

Zhao, Y., Pang, T., Du, C., Yang, X., Cheung, N.-M., and Lin, M. A recipe for watermarking diffusion models. *arXiv preprint arXiv:2303.10137*, 2023c.

Zhu, J., Kaplan, R., Johnson, J., and Fei-Fei, L. Hidden: Hiding data with deep networks. In *Proceedings of the European conference on computer vision (ECCV)*, pp. 657–672, 2018.

A. Watermarking Protection for Multiple Copyright Owners

As shown in Algorithm 1, to extend the protection from the one-owner case to the multiple-owner case, we first build the watermark protection for one owner and get the corresponding watermark decoder \mathcal{D}_θ (line 1). Then we use the same procedure (that can be decoded by \mathcal{D}_θ) to watermark all the images from other owners (lines 2 to 4).

Algorithm 1 Watermark protection for multiple copyright owners

Input: The number of distinct sets of images to protect, K . Distinct sets, $\{\mathbf{X}_{1:n}^k\}$ and different copyright messages for different owners \mathbf{M}^k , where $k = 1, 2, 3, \dots, K$.

Output: Watermarked images $\{\tilde{\mathbf{X}}_{1:n}^k\}$, where $k = 1, 2, 3, \dots, K$ and the watermark decoder \mathcal{D}_θ .

- 1: $\{\tilde{\mathbf{X}}_{1:n}^1\}, \mathcal{D}_\theta \leftarrow \text{OneOwnerCaseProtection}(\{\mathbf{X}_{1:n}^1\}, \mathbf{M}^1)$
 - 2: **for** $k = 2$ to K **do**
 - 3: $\{\tilde{\mathbf{X}}_{1:n}^k\} \leftarrow \text{ReuseEncodingProcess}(\{\mathbf{X}_{1:n}^k\}, \mathbf{M}^k)$
 - 4: **end for**
 - 5: return $\{\tilde{\mathbf{X}}_{1:n}^k\}, k = 1, 2, 3, \dots, K$ and \mathcal{D}_θ .
-

B. Theoretic Analysis on two examples

In this section, we use two examples, linear regression model and MLP, to show that watermarks with high pattern uniformity can be a stronger feature than others and can be learned easier/earlier than other features. We use MSE as the loss of linear regression and use a general loss in MLP to discuss a general case. We provide the theoretical examples in the two examples to explain that the watermarks with pattern uniformity can be learned prior to other features in the optimization starting at the initialized model.

B.1. Linear regression

Proof of Example 3.5. To reduce the loss by gradient descent, we derive the gradient of L with respect to \mathbf{w} :

$$\begin{aligned}
 \mathbb{E} \left[\frac{\partial L}{\partial \mathbf{w}} \right] &= \mathbb{E} \left[\frac{\partial (\tilde{\mathbf{Z}}^\top \mathbf{w} - \mathbf{S}^\top \boldsymbol{\beta} - \epsilon)^2}{\partial \mathbf{w}} \right] \\
 &= 2\mathbb{E} \left[\tilde{\mathbf{Z}} (\tilde{\mathbf{Z}}^\top \mathbf{w} - \mathbf{S}^\top \boldsymbol{\beta} - \epsilon) \right] \\
 &= 2\mathbb{E} \left[\tilde{\mathbf{Z}} (\tilde{\mathbf{Z}}^\top \mathbf{w}) \right] - 2\mathbb{E} \left[\tilde{\mathbf{Z}} (\mathbf{S}^\top \boldsymbol{\beta} + \epsilon) \right] \\
 &= 2\mathbb{E} \left[(\mathbf{M}\mathbf{S} + \boldsymbol{\delta})(\mathbf{M}\mathbf{S} + \boldsymbol{\delta})^\top \mathbf{w} \right] - 2\mathbb{E} \left[(\mathbf{M}\mathbf{S} + \boldsymbol{\delta})(\mathbf{S}^\top \boldsymbol{\beta} + \epsilon) \right] \\
 &= 2(\mathbb{E} \left[\mathbf{M}\mathbf{S}\mathbf{S}^\top \mathbf{M}^\top \right] + \mathbb{E} \left[\boldsymbol{\delta}\boldsymbol{\delta}^\top \right])\mathbf{w} - 2(\mathbb{E} \left[\mathbf{M}\mathbf{S}\mathbf{S}^\top \boldsymbol{\beta} \right] + \mathbb{E} \left[\boldsymbol{\delta}\mathbf{S}^\top \boldsymbol{\beta} \right]) - 2\mathbb{E} \left[(\mathbf{M}\mathbf{S} + \boldsymbol{\delta})\epsilon \right] \\
 &= 2(\mathbb{E} \left[\mathbf{M}\mathbf{S}\mathbf{S}^\top \mathbf{M}^\top \right] + \mathbb{E} \left[\boldsymbol{\delta}\boldsymbol{\delta}^\top \right])\mathbf{w} - 2\mathbb{E} \left[\mathbf{M}\mathbf{S}\mathbf{S}^\top \boldsymbol{\beta} \right].
 \end{aligned} \tag{6}$$

In the above gradient, we separate the hidden feature term according to whether it contains \mathbf{w} to make the comparison with terms with and without \mathbf{w} in watermark term.

For $(\mathbb{E} \left[\mathbf{M}\mathbf{S}\mathbf{S}^\top \mathbf{M}^\top \right] + \mathbb{E} \left[\boldsymbol{\delta}\boldsymbol{\delta}^\top \right])\mathbf{w}$, we transform the gradient by \mathbf{M}^\top to compare the influence on \mathbf{S} by each dimension s_i . The norm of the two terms are

$$\begin{aligned}
 \left(\mathbf{M}^\top \mathbb{E} \left[\mathbf{M}\mathbf{S}\mathbf{S}^\top \mathbf{M}^\top \right] \mathbf{w} \right)_i &= \left(\mathbb{E} \left[\mathbf{S}\mathbf{S}^\top \right] \mathbf{M}^\top \mathbf{w} \right)_i \\
 &= \mathcal{O} \left(\frac{1}{d} \left\| \mathbf{M}_i^\top \mathbf{w} \right\| \right) \\
 &= \mathcal{O}_p \left(\frac{1}{d} \right),
 \end{aligned} \tag{7}$$

and

$$\left\| \mathbf{M}^\top \mathbb{E} [\delta \delta^\top \mathbf{w}] \right\| = \left\| \mathbb{E} [\delta \delta^\top \mathbf{w}] \right\| = \|\mathbb{E}[\delta]\| \times \mathcal{O}(\|\delta\|) = \mathcal{O}(\|\delta\|^2). \quad (8)$$

When $\|\delta\| \gg 1/\sqrt{d}$, the norm of the watermark term in Eq. 8 is larger than the gradient term from each hidden feature in Eq. 7, which means the watermark feature is learned prior to other hidden features in the first optimization step after model is random initialized.

Similarly, for the rest part in the gradient of Eq. 6, we have

$$\left(\mathbf{M}^\top \mathbb{E} [\mathbf{M} \mathbf{S} \mathbf{S}^\top \beta] \right)_i = \mathcal{O} \left(\frac{1}{d} (\mathbf{I}_d \beta)_i \right) = \mathcal{O} \left(\frac{1}{d} \beta_i \right) = \mathcal{O} \left(\frac{1}{d} \right). \quad (9)$$

When $\|\delta\| \gg 1/\sqrt{d}$, the watermark term in Eq. 8 will have a larger norm than Eq. 9 and the watermark feature can be learned prior to other features.

Combining the other side, when $1/\sqrt{d} \ll \|\delta\| \ll 1/\sqrt{pd}$, because of pattern uniformity, the watermark will have more influence and be learned prior to other hidden features after random initialization even though the watermark has a much smaller norm than each active hidden feature.

On the other hand, assume the watermark δ has a worse pattern uniformity, and δ is independent with \mathbf{Z} . Then the sum of all eigenvalues $\lambda_i(\mathbb{E}[\delta \delta^\top])$ is unchanged, i.e.,

$$\sum_i \lambda_i(\mathbb{E}[\delta \delta^\top]) = \text{tr} \left(\mathbb{E}[\delta \delta^\top] \right) = \mathbb{E} \text{tr}[\delta \delta^\top] = \mathbb{E} \|\delta\|^2.$$

However, since δ is random, there are more λ_i s which are not zero. Consequently, if we look at the $\left\| \mathbb{E} [\delta \delta^\top \mathbf{w}] \right\|$, we study

$$\mathbb{E}_{\mathbf{w}} \left\| \mathbb{E}_{\delta} [\delta \delta^\top \mathbf{w}] \right\|^2 = \text{tr} \left(\mathbb{E}[\delta \delta^\top] \mathbb{E}[\delta \delta^\top] \right) = \sum_i \lambda_i(\mathbb{E}[\delta \delta^\top])^2,$$

and then we can find that the average $\left\| \mathbb{E} [\delta \delta^\top \mathbf{w}] \right\|$ becomes smaller.

On the other hand, it is also easy to figure out that the best \mathbf{w} to minimize L is

$$\mathbf{w}^* = (\mathbf{I}_d + \mathbb{E} \epsilon \epsilon^\top + \delta \delta^\top)^{-1} \mathbf{M} \beta,$$

i.e., the training process does not forget δ in the end. □

B.2. Neural Network with a General Task

Remark B.1. While one can obtain a closed-form solution in Example 3.5 for linear regression problem, in Example 3.5, there is no closed-form solution of the trained neural network. Although theoretically tracking the behavior of the neural network is beyond our scope, we highlight that in existing theoretical studies, e.g., (Ba et al., 2019; Allen-Zhu & Li, 2022), the neural network will not forget any learned features during the training.

Proof of Example 3.5. We denote one of the neurons in \mathcal{W}_1 as \mathbf{w}_h and shorten the notation of $L(\mathcal{W}, \mathbf{S})$ as L . In the following, we proof that the gradient updating of each neuron in the first layer is dominated by the δ because the watermark term has a larger norm compared with other hidden features.

We first derive the gradient of L with respect to \mathbf{w}_h :

$$\frac{\partial L}{\partial \mathbf{w}_h} = \frac{\partial L}{\partial \mathbf{w}_h^\top \tilde{\mathbf{Z}}} \frac{\partial \mathbf{w}_h^\top \tilde{\mathbf{Z}}}{\partial \mathbf{w}_h} = \frac{\partial L}{\partial \mathbf{w}_h^\top \tilde{\mathbf{Z}}} \tilde{\mathbf{Z}} = \frac{\partial L}{\partial \mathbf{w}_h^\top \tilde{\mathbf{Z}}} (\mathbf{M} \mathbf{S} + \delta).$$

By denoting $\frac{\partial L}{\partial \mathbf{w}_h^\top \tilde{\mathbf{Z}}}$ as $\rho(\tilde{\mathbf{Z}})$, we get

$$\frac{\partial L}{\partial \mathbf{w}_h} = \rho(\tilde{\mathbf{Z}}) (\mathbf{M} \mathbf{S} + \delta).$$

For simplicity, we assume $M = \mathbf{I}_d$. Then the gradient is

$$\frac{\partial L}{\partial \mathbf{w}_h} = \rho(\tilde{\mathbf{Z}}) (\mathbf{S} + \delta).$$

To compare the norm of gradient related to x_i with watermark term, we define $\mathbf{S}_{-i} = (\mathbf{s}_1, \dots, \mathbf{s}_{i-1}, 0, \mathbf{s}_{i+1}, \dots, \mathbf{s}_d)$, and $\mathbf{S}_i = (0, \dots, 0, \mathbf{s}_i, 0, \dots, 0)$. Then

$$\begin{aligned} \frac{\partial L}{\partial \mathbf{w}_h} &= \rho(\tilde{\mathbf{Z}}) (\mathbf{S}_{-i} + \mathbf{S}_i + \delta) \\ &= \rho(\mathbf{S}_{-i} + \mathbf{S}_i + \delta) (\mathbf{S}_{-i} + \mathbf{S}_i + \delta) \\ &= \left[\rho(\mathbf{S}_{-i}) + \rho'(\mathbf{S}_{-i})^\top (\mathbf{S}_i + \delta) + \frac{1}{2} \|\mathbf{S}_i + \delta\|_{\rho''(\mathbf{S}_{-i})}^2 + \mathcal{O}(\|\mathbf{S}_i + \delta\|^3) \right] (\mathbf{S}_{-i} + \mathbf{S}_i + \delta) \\ &= \rho(\mathbf{S}_{-i}) (\mathbf{S}_{-i} + \mathbf{S}_i + \delta) + \rho'(\mathbf{S}_{-i})^\top (\mathbf{S}_i + \delta) (\mathbf{S}_{-i} + \mathbf{S}_i + \delta) \\ &\quad + \frac{1}{2} \|\mathbf{S}_i + \delta\|_{\rho''(\mathbf{S}_{-i})}^2 \mathbf{S}_{-i} + \mathcal{O}(\|\mathbf{S}_i + \delta\|^3) \\ &= \rho(\mathbf{S}_{-i}) \mathbf{S}_{-i} + \rho'(\mathbf{S}_{-i})^\top (\mathbf{S}_i + \delta) \mathbf{S}_{-i} \\ &\quad + \rho(\mathbf{S}_{-i}) (\mathbf{S}_i + \delta) + \rho'(\mathbf{S}_{-i})^\top (\mathbf{S}_i + \delta) (\mathbf{S}_i + \delta) + \frac{1}{2} \|\mathbf{S}_i + \delta\|_{\rho''(\mathbf{S}_{-i})}^2 \mathbf{S}_{-i} \\ &\quad + \mathcal{O}(\|\mathbf{S}_i + \delta\|^3). \end{aligned}$$

We further assume $\mathbb{E}\rho(\mathbf{S}_{-i}) = 0$, $\mathbb{E}\rho'(\mathbf{S}_{-i})\mathbf{S}_{-i}^\top = 0$, $\mathbb{E}\rho'(\mathbf{S}_{-i})^\top \delta = \Theta(\|\delta\| \|\mathbb{E}\rho'(\mathbf{S}_{-i})\|)$, and $\|\mathbb{E}\|\mathbf{a}\|_{\rho''(\mathbf{S}_{-i})}^2 \mathbf{S}_{-i}\| = \Theta(\|\mathbf{a}\| \|\mathbb{E}\rho'(\mathbf{S}_{-i})\|)$ for any proper vector \mathbf{a}^1 . Taking the expectation of the gradient,

$$\begin{aligned} \mathbb{E}_{\mathbf{S}} \left[\frac{\partial L}{\partial \mathbf{w}_h} \right] &= \underbrace{\mathbb{E}\rho(\mathbf{S}_{-i})\mathbf{S}_{-i}}_{=0} + \underbrace{\mathbb{E}\rho'(\mathbf{S}_{-i})^\top \mathbf{S}_{-i}(\mathbf{S}_i + \delta)}_{=0} \\ &\quad + \underbrace{\mathbb{E}\rho(\mathbf{S}_{-i})(\mathbf{S}_i + \delta)}_{=0} + \mathbb{E}\rho'(\mathbf{S}_{-i})^\top (\mathbf{S}_i + \delta) (\mathbf{S}_i + \delta) + \mathbb{E}\frac{1}{2} \|\mathbf{S}_i + \delta\|_{\rho''(\mathbf{S}_{-i})}^2 \mathbf{S}_{-i} \\ &\quad + \underbrace{\mathcal{O}(\|\mathbf{S}_i + \delta\|^3)}_{\text{negligible}} \\ &= \mathbb{E}(\mathbf{S}_i + \delta) (\mathbf{S}_i + \delta)^\top \mathbb{E}\rho'(\mathbf{S}_{-i}) + \mathbb{E}\frac{1}{2} \|\mathbf{S}_i + \delta\|_{\rho''(\mathbf{S}_{-i})}^2 \mathbf{S}_{-i} + o \\ &= \left(\mathbb{E}\mathbf{S}_i \mathbf{S}_i^\top + \delta \delta^\top \right) \mathbb{E}\rho'(\mathbf{S}_{-i}) + \frac{1}{2} \mathbb{E}\mathbf{S}_{-i} \left(\mathbb{E}\mathbf{S}_i \|\mathbf{S}_i\|_{\rho''(\mathbf{S}_{-i})}^2 + \|\delta\|_{\rho''(\mathbf{S}_{-i})}^2 \right) \mathbf{S}_{-i} + o. \end{aligned}$$

The notation o represents negligible terms.

Since $\mathbb{E}\rho'(\mathbf{S}_{-i})^\top \delta = \Theta(\|\delta\| \|\mathbb{E}\rho'(\mathbf{S}_{-i})\|)$, when $\|\delta\| \gg \mathbb{E}[\mathbf{S}_i]$, we have

$$\left\| \left(\mathbb{E}\mathbf{S}_i \mathbf{S}_i^\top \right) \mathbb{E}\rho'(\mathbf{S}_{-i}) \right\| \ll \left\| \left(\delta \delta^\top \right) \mathbb{E}\rho'(\mathbf{S}_{-i}) \right\|.$$

On the other hand, since $\|\mathbb{E}\|\mathbf{a}\|_{\rho''(\mathbf{S}_{-i})}^2 \mathbf{S}_{-i}\| = \Theta(\|\mathbf{a}\| \|\mathbb{E}\rho'(\mathbf{S}_{-i})\|)$, when $\|\delta\| \gg \mathbb{E}[\mathbf{S}_i]$, we have

$$\left\| \mathbb{E}\mathbf{S}_{-i} \left(\mathbb{E}\mathbf{S}_{-i} \|\mathbf{S}_i\|_{\rho''(\mathbf{S}_{-i})}^2 \right) \mathbf{S}_{-i} \right\| \ll \left\| \mathbb{E}\mathbf{S}_{-i} \left(\|\delta\|_{\rho''(\mathbf{S}_{-i})}^2 \right) \mathbf{S}_{-i} \right\|.$$

To summarize, in general, when $\|\delta\| \gg \mathbb{E}[\mathbf{S}_i]$, i.e. $\|\delta\| \gg 1/\sqrt{d}$, the norm of the watermark term in the gradient will be much larger than than expectation of any hidden feature, which means the watermark will be learned prior to other features.

The effect of uniformity of δ follows the same as in Example 3.5. □

¹To simplify the analysis, we directly connect $\|\mathbb{E}\|\mathbf{a}\|_{\rho''(\mathbf{S}_{-i})}^2 \mathbf{S}_{-i}\|$ to $\|\mathbf{a}\|$. To relax this condition, one may consider imposing proper assumptions to exactly derive the formula of $\|\mathbb{E}\|\mathbf{a}\|_{\rho''(\mathbf{S}_{-i})}^2 \mathbf{S}_{-i}\|$. We also avoid extreme cases where terms cancel with each other, e.g., $\delta \delta^\top \mathbb{E}\rho'(\mathbf{S}_{-i}) = -\mathbb{E}\mathbf{S} \|\delta\|_{\rho''(\mathbf{S}_{-i})}^2 \mathbf{S}_{-i}/2$

B.3. Experiment to Support Theoretic Analysis with the Two Examples

We use DDPM to learn a watermarked *bird* class in CIFAR10 and compare the accuracy and the quality of generated images in different steps of the training process. The results in Figure 6 show that watermark is much earlier learned before the semantic features, which is consistent with our theoretic analysis in the two examples. In Figure 6, we can see that, at step 20k, the watermark accuracy in generated images is already 94%, but the generated image has no visible feature of bird at all. The bird is generated in high quality until step 60k. This means the watermark is learned much earlier than the semantic features of the images. The observation aligns with our theoretic analysis.

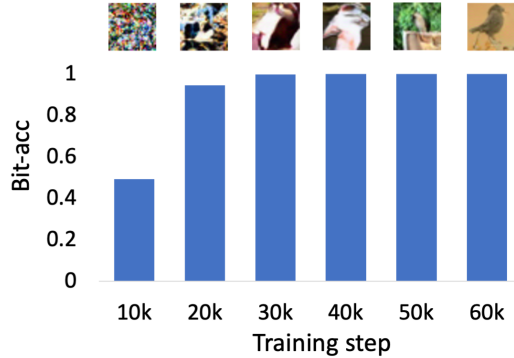


Figure 6. The change of bit accuracy and generated images in the training process.

C. Additional Details of Experimental Settings

C.1. Watermarks and Detector of Experiment for Pattern Uniformity in Section 3.2

In the experiment shown in Figure 3, we test the ability of DDPM (Ho et al., 2020) to learn watermarks with different pattern uniformity and show more details about the setting in this subsection.

Watermarks. We first choose one class from CIFAR10 as images requiring watermarks $\mathbf{X}_{1:R}$, where R is the number of images in this class and $R = 5000$ for CIFAR10. We randomly choose C images from 5 classes from CIFAR10 as $\mathbf{W}_{1:C}$, where C is the number of different watermarks and $C = 5, 10, 15, \dots$. Different watermarks are repeatedly added into $\mathbf{X}_{1:R}$ by $\tilde{\mathbf{X}}_i = \mathbf{X}_i + \sigma \times \mathbf{W}_i$. For example, we choose $C = 10$ images as watermarks and every watermark is used to watermark $R/C = 500$ images in $\mathbf{X}_{1:R}$. By choosing different C , we can control the uniformity. Larger C means more diverse watermarks and thus smaller pattern uniformity.

Detector. We train a classifier as the detector to detect the watermark in the generated images. The classifier is trained on the images watermarked by 10 classes. The label of the training images is set to be the watermark class. If the classifier predicts that the GDM-generated images have the watermark within the 5 classes from which the C watermarks are chosen, we see it as a successful detection, otherwise it is unsuccessful.

C.2. Block size and message length for different datasets

In our experiment, we considered four datasets, including CIFAR10 and CIFAR100, both with $(U, V) = (32, 32)$, STL10 with $(U, V) = (64, 64)$ and ImageNet-20 with $(U, V) = (256, 256)$. For CIFAR10, CIFAR100 and STL10, we consider the block size $(u, v) = (4, 4)$ and $B = 4$. For ImageNet-20, we set $(u, v) = (16, 16)$ and $B = 2$. Therefore, for CIFAR10 and CIFAR100, we are able to encode $\binom{32}{4} \times \binom{32}{4} \times 2 = 128$ bit. For STL-10, we can embed $\binom{64}{4} \times \binom{64}{4} \times 2 = 512$ bit. And for ImageNet, the message length is $\binom{256}{16} \times \binom{256}{16} = 256$ bits.

C.3. Decoder Architecture and Details about Training Parameters.

Given the small size of the blocks (4×4) , we adapt the original ResNet structure by including only two residual blocks with 64 filters each, positioned between the initial convolutional layer and the global average pooling layer. In the joint optimization, for training decoder, we use the SGD optimizer with momentum to be 0.9, learning rate to be 0.01 and weight decay to be 5×10^{-4} , while for training watermark basic patches, we use 5-step PGD with step size to be 1/10 of the L_∞

budget.

C.4. Details of Baselines

Our method is compared with four existing watermarking methods although they are not specifically designed for the protection of image copyright against GDMs. Information on the baseline methods is provided as follows:

- **Image Blending (IB)**, a simplified version of our approach, which also applies blockwise watermark to achieve pattern uniformity but the patches are not optimized. Instead, it randomly selects some natural images, re-scales their pixel values to 8/255, and uses these as the basic patches. A trained classifier is also required to distinguish which patch is added to a block.
- **DWT-DCT-SVD based watermarking (FRQ)**, one of the traditional watermarking schemes based on the frequency domains of images. It uses Discrete Wavelet Transform (DWT) to decompose the image into different frequency bands, Discrete Cosine Transform (DCT) to separate the high-frequency and low-frequency components of the image, and Singular Value Decomposition (SVD) to embed the watermark by modifying the singular values of the DCT coefficients.
- **HiDDeN (Zhu et al., 2018)**, a neural network-based framework for data hiding in images. The model comprises a network architecture that includes an encoding network to hide information in an image, a decoding network to extract the hidden information from the image, and a noise network to attack the system, making the watermark robust. In our main experiments, we did not incorporate noise layers into HiDDeN, except during tests of its robustness to noise (Experiments in 4.6).
- **DeepFake Fingerprint Detection (DFD) (Yu et al., 2021)**, a method for Deepfake detection and attribution (trace the model source that generated a deepfake). The fingerprint is developed as a unique pattern or signature that a generative model leaves on its outputs. It also employs an encoder and a decoder, both based on Convolutional Neural Networks (CNNs), to carry out the processes of watermark embedding and extraction.

C.5. Comparison to Additional Baselines

We have conducted a comparison of our method with three other baselines: IGA (Zhang et al., 2020a), MBRS (Jia et al., 2021), and CIN (Ma et al., 2022). The results are reported in Table 5 and 6 below. We can see that the performance of IGA is very similar to HiDDeN and DFD. Although IGA’s bit accuracy is comparable to our DiffusionShield, it demands a significantly higher budget—more than 20 times the L_∞ and LPIPS values of our approach. As for MBRS and CIN, despite having budgets lower than IGA, they exhibit a worse trade-off between budget and bit accuracy compared to our method, especially on CIFAR100. Specifically, MBRS only attains an 87.68% bit accuracy at twice our budget, and CIN only achieves a 51.13% bit accuracy with a budget close to ours. In contrast, DiffusionShield maintains a high bit accuracy of 99.80% without necessitating a high budget. This is because of the higher pattern uniformity of DiffusionShield. In summary, the performances of these baselines are similar to the previous baseline methods. They either compromise the budget for bit accuracy close to ours, or fail to be reproduced well in the generated images.

Table 5. Comparison to Additional Baselines with CIFAR-10

| Metric | IGA | MBRS | CIN | Ours | |
|------------|---------|---------|---------|----------------|---------------|
| L_∞ | 52/255 | 16/255 | 8/255 | 1/255 | 2/255 |
| L2 | 3.38 | 0.36 | 0.42 | 0.18 | 0.36 |
| LPIPS | 0.08910 | 0.00182 | 0.00185 | 0.00005 | 0.00020 |
| Cond. Acc. | 99.63% | 99.97% | 99.97% | 99.90% | 99.99% |
| Uniformity | 0.063 | 0.518 | 0.599 | 0.974 | 0.971 |

Table 6. Comparison to Additional Baselines with CIFAR-100

| Metric | IGA | MBRS | CIN | Ours | |
|------------|---------|-------------|----------------|--------------|---------------|
| L_∞ | 66/255 | 19/255 | 9/255 | 4/255 | 8/255 |
| L2 | 5.31 | 0.43 | 0.44 | 0.72 | 1.43 |
| LPIPS | 0.08830 | 0.00129 | 0.00105 | 0.00134 | 0.00672 |
| Cond. Acc. | 97.25% | 87.68% | 51.13% | 99.80% | 99.99% |
| Uniformity | 0.162 | 0.394 | 0.527 | 0.836 | 0.816 |

C.6. Standard DDPM and Improved DDPM.

Standard DDPM. Denoising Diffusion Probabilistic Model (DDPM), firstly developed by (Ho et al., 2020), consists of a diffusion process $q(x_t | x_{t-1})$ and a denoising process $p_\theta(x_{t-1} | x_t)$ which are respectively described as:

$$q(x_t | x_{t-1}) = \mathcal{N}(x_t; \sqrt{1 - \beta_t}x_{t-1}, \beta_t I) \quad (10)$$

$$p_\theta(x_{t-1} | x_t) = \mathcal{N}(x_{t-1}; \mu_\theta(x_t, t), \Sigma_\theta(x_t, t)) \quad (11)$$

With the variance schedule β_t , a data point x_0 sampled from a real data distribution is transformed into noise x_T by continuously adding a small amount of Gaussian noise to the sample for T steps. Then the image is gradually reconstructed by removing the noise from x_T following the reverse diffusion process 11.

The most effective way to parameterize $\mu_\theta(x_t, t)$ is to predict the noise added to x_0 in each step with a neural network. In practice, we use the simplified objective suggested by (Ho et al., 2020)

$$L_t^{\text{simple}} = \mathbb{E}_{t \sim [1, T], x_0, \epsilon_t} \left[\left\| \epsilon_t - \epsilon_\theta(\sqrt{\alpha_t}x_0 + \sqrt{1 - \alpha_t}\epsilon_t, t) \right\|^2 \right]$$

Then the denoising process can be described as:

$$x_{t-1} = \frac{1}{\sqrt{\alpha_t}} \left(x_t - \frac{1 - \alpha_t}{\sqrt{1 - \alpha_t}} \epsilon_\theta(x_t, t) \right) + \sigma_t \mathbf{z}$$

Improved DDPM. (Nichol & Dhariwal, 2021) proposed a few modifications of DDPM to achieve faster sampling speed and better log-likelihoods. The primary modification is to turn $\Sigma_\theta(x_t, t)$ into a learned function using the formula

$$\Sigma_\theta(x_t, t) = \exp \left(v \log \beta_t + (1 - v) \log \tilde{\beta}_t \right).$$

Moreover, they proposed a hybrid training objective

$$L_{\text{hybrid}} = L_t^{\text{simple}} + \lambda L_{\text{vlb}}$$

where L_{vlb} refers to the variational lower-bound of DDPM. To reduce the variance of the training log loss of L_{vlb} , they proposed importance sampling:

$$L_{\text{vlb}} = E_{t \sim p_t} \left[\frac{L_t}{p_t} \right], \text{ where } p_t \propto \sqrt{E[L_t^2]} \text{ and } \sum p_t = 1$$

Finally, they introduced an enhancement to the noise schedule with:

$$\bar{\alpha}_t = \frac{f(t)}{f(0)}, \quad f(t) = \cos \left(\frac{t/T + s}{1 + s} \cdot \frac{\pi}{2} \right)^2$$

D. Algorithm

As shown in Algorithm 2, the joint optimization is numerically solved by alternately training on the two levels. Every batch is first watermarked and trained on the classifier for upper level objective by gradient descent (line 4 to 6), and then optimized on basic patches for lower level objective by 5-step PGD (line 7 to 9). With the joint optimized basic patches and classifier, we can obtain a robust watermark that can encode different ownership information with a small change on the protected data. This watermark can be easily captured by the diffusion model and is effective for tracking data usage and copyright protection. The clean images $\{\mathbf{X}_{1:n}\}$ for input of the algorithm is not necessary to be the images that we want to protect. The random cropped image blocks can help the basic patches to fit different image blocks and then increase the flexibility.

Algorithm 2 Joint optimization on $\{\mathbf{w}^{(1:B)}\}$ and \mathcal{D}_θ

Input: Initialized basic patches $\{\mathbf{w}_{(0)}^{(1:B)}\}$, clean images $\{\mathbf{X}_{1:n}\}$, upper and lower level objectives in Eq. 3, $\mathcal{L}_{\text{upper}}$, $\mathcal{L}_{\text{lower}}$, watermark budget ϵ , decoder learning rate r , batch size bs , PGD step α and epoch E .

Output: Optimal $\{\mathbf{w}^{(1:B),*}\}$ and θ^* .

```

1:  $step \leftarrow 0$ 
2: for  $epoch=1$  to  $E$  do
3:   for  $Batch$  from  $\{\mathbf{X}_{1:n}\}$  do
4:      $\{\mathbf{p}_{1:bs}\} \leftarrow \text{RandomCropBlock}(Batch)$ 
5:      $\{\mathbf{w}_{1:bs}\}, \{\mathbf{b}_{1:bs}\} \leftarrow \text{RandomPermutation}(\{\mathbf{w}_{(step)}^{(1:B)}\}, bs)$ 
6:      $\theta \leftarrow \text{StochasticGradientDescent}(\frac{\partial \sum_1^{bs} \mathcal{L}_{\text{lower}}(\mathbf{p}_i + \mathbf{w}_i, \mathbf{b}_i, \theta)}{\partial \theta}, r)$  // Training on classifier
7:     for 1 to 5 do
8:        $\mathbf{w}_{(step)}^{(2:B)} \leftarrow \text{Clip}_{(-\epsilon, \epsilon)} \left( \mathbf{w}_{(step)}^{(2:B)} - \alpha \text{sign} \left( \frac{\partial \sum_1^{bs} \mathcal{L}_{\text{lower}}(\mathbf{p}_i + \mathbf{w}_i, \mathbf{b}_i, \theta)}{\partial \mathbf{w}_{(step)}^{(2:B)}} \right) \right)$  // 5-step Projected Gradient Descent
9:     end for
10:     $step \leftarrow step + 1$ 
11:  end for
12:  return  $\{\mathbf{w}_{(step)}^{(1:B)}\}$  and  $\theta$ .
13: end for
    
```

E. Examples of Watermarked Images

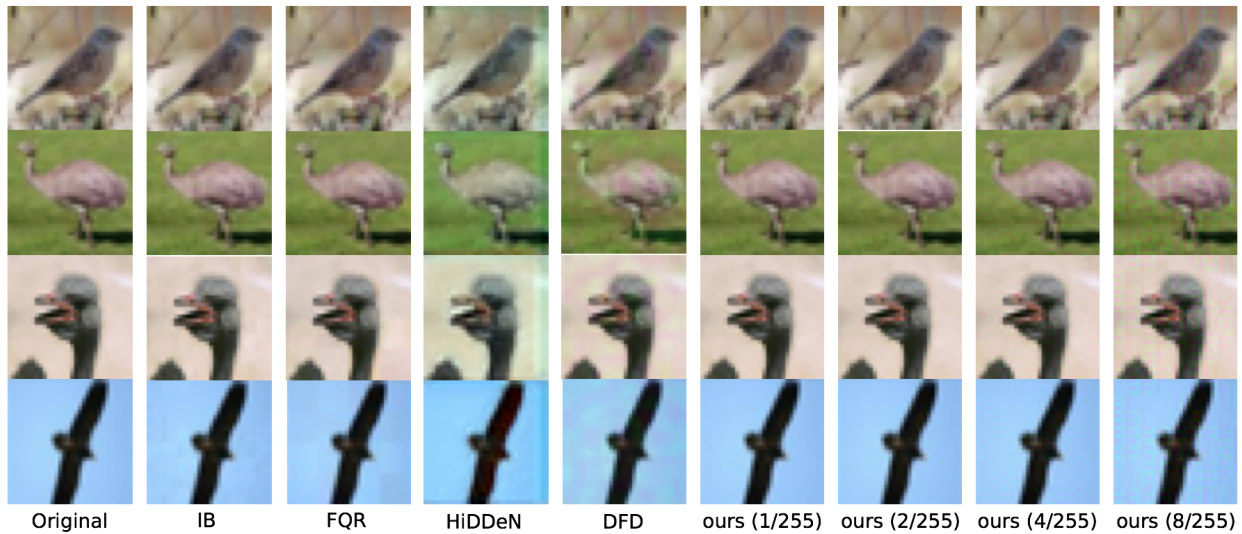


Figure 7. Examples of watermarked images of the bird class in CIFAR-10

DiffusionShield: A Watermark for Data Copyright Protection against Generative Diffusion Models

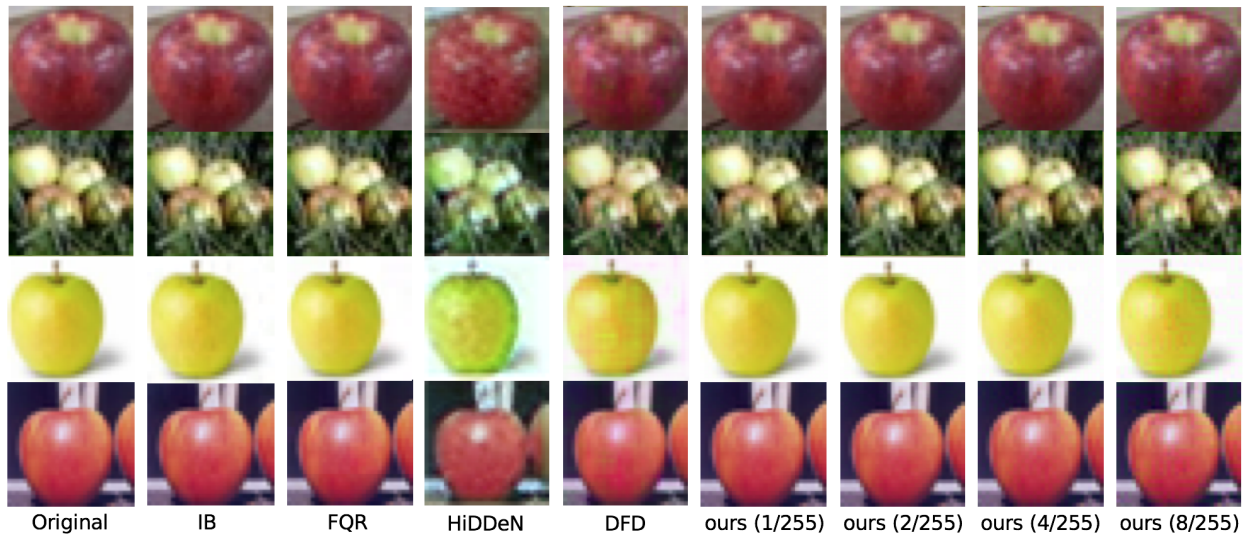


Figure 8. Examples of watermarked images of the apple class in CIFAR-100



Figure 9. Examples of watermarked images of the plane class in STL-10

F. Additional Analysis on the Influence of Budget and Watermark Rate

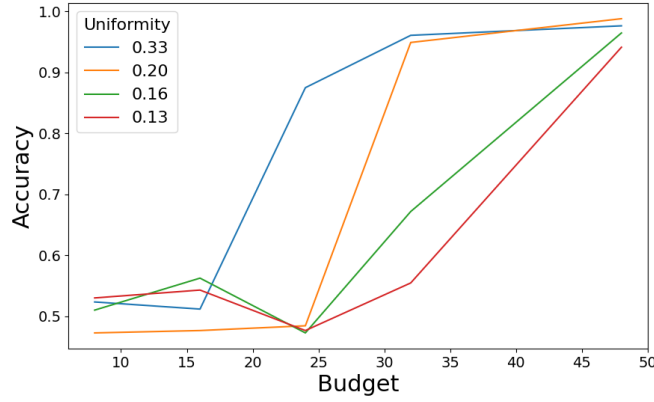


Figure 10. The change of bit accuracy under different budgets

As mentioned in Section 4.2, the reproduction of watermarks in generated images is related to the watermark budget and the watermark rate. In this subsection, we show that a larger budget and larger watermark rate can help with the reproduction of watermarks in the GDM-generated images.

In Figure 10, we follow the experimental setting in Section 3.2. We can see that when uniformity is the same, as the budget increases, the detection rate is also increasing, which means that watermarks can reproduce better if it has a larger budget. This can also be observed from Table 4.2 that the bit accuracy of budget 1/255 and 2/255 on CIFAR100 is lower than 4/255 and 8/255. Meanwhile, higher pattern uniformity can increase faster than lower pattern uniformity, which is consistent with Section 3.2.

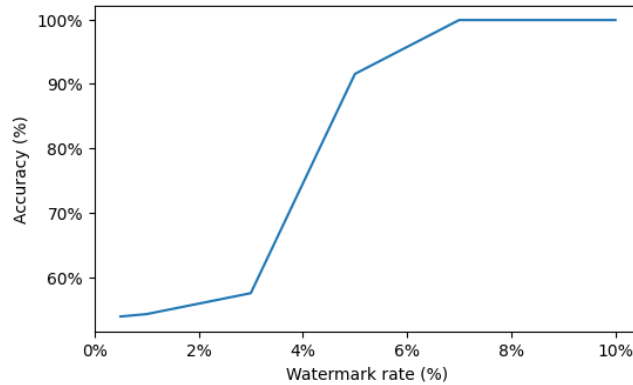


Figure 11. The change of bit accuracy with different watermark rates (budget=1/255)

In Figure 11, we follow the experimental setting in Section 4.1, while controlling the proportion of the watermarked images in the training set of GDM. From the figure, we can see that the bit accuracy on the generated images rises from about 53% to almost 100% when the watermark rate increases from 0.05% to 10%, which indicates that the watermark rate can affect the degree of reproduction of the watermark in generated images.

Figure 11 suggests that DiffusionShield cannot provide satisfied protection in the single-owner case when the watermark rate and the budget are small. In reality, the watermark rate for a single user may be small. However, there are multiple users who may adopt DiffusionShield to protect the copyright of their data. Therefore, next we check how the performance of DiffusionShield changes with the number of users when the watermark rate and the budget are small for each user. Although each user has a distinct set of watermarked data, they all share the same set of basic patches, which has the potential to enhance the reproducibility of the watermark. As shown in Figure 12, we have K owners and the images of each owner

Table 7. Bit accuracy (%) with speeding-up models

| l_∞ | | CIFAR10 | CIFAR100 | STL10 |
|------------|---------|----------|----------|---------|
| 1/255 | Cond. | 99.7824 | 52.4813 | 95.8041 |
| | Uncond. | 94.6761 | 52.2693 | 82.4564 |
| 2/255 | Cond. | 99.9914 | 64.5070 | 99.8299 |
| | Uncond. | 96.1927 | 53.4493 | 90.4317 |
| 4/255 | Cond. | 99.9996 | 99.8445 | 99.9102 |
| | Uncond. | 96.1314 | 92.3109 | 95.7027 |
| 8/255 | Cond. | 100.0000 | 99.9984 | 99.9885 |
| | Uncond. | 95.7021 | 92.2341 | 95.3009 |

compose 1% of the collected training data. As the number of owners increases from 1 to 20, the average accuracy increases from about 64% to nearly 100%. This observation indicates that DiffusionShield can work with multiple users even when the watermark rate and the budget are small for each user. Since GDM often collects training data from multiple users, this study suggests that DiffusionShield could be very practical.

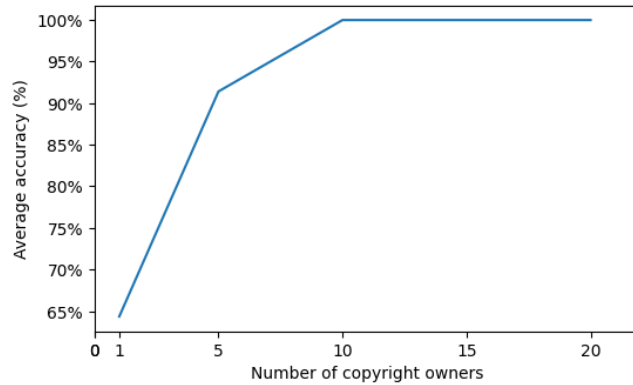


Figure 12. The change of bit accuracy with different numbers of copyright owners (budget=2/255)

G. Details of Experiments on Robustness & Additional Evaluation

G.1. Details of the Settings of the Corruption Considered in Section 4.6

- Gaussian noise: The mean of the noise is set to 0 the standard deviation is set to 0.1.
- Low-pass Filter: The kernel size of the low-pass filtering is set to 5 and the sigma is 1.
- JPEG Compression: The quality of JPEG Compression is set to 80%.
- Resize: We altered image sizes from 32x32 to 64x64 (termed “large” in the Table 4), or from 32x32 to 16x16 (termed “small” in the table). During detection, we resize all the data back to 32x32 before inputting them to the detector.

G.2. Robustness under Speeding-up Sampling Models

Speeding-up sampling is often employed by practical GDMs due to the time-consuming nature of the complete sampling process, which requires thousands of steps. However, the quality of the images generated via speeded-up methods, such as Denoising Diffusion Implicit Model (DDIM) (Song et al., 2020), is typically lower than normal sampling, which could destroy the watermarks on the generated images. In Table 7, we show the performance of DiffusionShield with DDIM to demonstrate its robustness against speeding-up sampling. Although DiffusionShield has low accuracy on CIFAR100 when the budget is 1/255 and 2/255 (same as the situation in Section 4.2), it can maintain high accuracy on all the other budgets and datasets. Even with a 1/255 l_∞ budget, the accuracy of DiffusionShield on CIFAR10 is still more than 99.7% in class-conditionally generated images and more than 94.6% in unconditionally generated images. This is because the

easy-to-learn uniform patterns are learned by GDMs prior to other diverse semantic features like shape and textures. Thus, as long as DDIM can generate images with normal semantic features, our watermark can be reproduced in these images.

G.3. Robustness under Different Hyper-parameters in Training GDMs

Besides the speeded up sampling method, we test two more hyperparameters in Table 8 below. They are learning rate and diffusion noise schedule. Diffusion noise schedule is a hyperparameter that controls how the gaussian noise added into the image increases during the diffusion process. We test with two different schedules, cosine and linear. We use DiffusionShield with 2/255 budget to protect one class in CIFAR10. The results show that the watermark accuracies in all the different parameters are higher than 99.99%, which means our method is robust under different diffusion model hyperparameters.

Table 8. Bit accuracy under different hyper-parameters of DDPM

| | cosine | linear |
|------|----------|----------|
| 5e-4 | 99.9985% | 99.9954% |
| 1e-4 | 99.9945% | 99.9908% |
| 1e-5 | 99.9939% | 99.9390% |

H. Details of Generalization to Fine-tuning GDMs

In Table 9 and Table 10, we measure the generated quality of both watermarked class and all classes to show that DiffusionShield will not influence the quality of generated images. We use FID to measure the quality of generated images. Lower FID means better generated quality. Comparing FIDs of watermarked classes by different watermark methods, we can find that our method can keep a smaller FID than DFD and HiDDeN when the budget is smaller than 4/255. This means our watermark is more invisible. Comparing FID of ours and clean data, we can find that our method has almost no influence on the generated quality of GDMs. We can also see that FID for the watermarked class is usually higher than FID for all the classes. This is because FID is usually larger when the sample size is small and we sample fewer images in watermarked class than the total number of the samples from all the classes. In summary, our method will not influence the quality of generated images.

Table 9. Bit accuracy under different hyper-parameters of DDPM

| method | clean | ours(1/255) | ours(4/255) | ours(8/255) | DFD | HiDDeN |
|--------|--------|-------------|-------------|-------------|--------|--------|
| FID | 15.633 | 14.424 | 26.868 | 51.027 | 33.884 | 48.939 |

Table 10. Bit accuracy under different hyper-parameters of DDPM

| method | clean | ours(1/255) | ours(4/255) | ours(8/255) |
|--------|-------|-------------|-------------|-------------|
| FID | 3.178 | 4.254 | 3.926 | 4.082 |

I. Details of Generalization to Fine-tuning GDMs

Background in fine-tuning GDMs. To speed up the generation of high-resolution image, Latent Diffusion Model proposes to project the images to a vector in the hidden space by a pre-trained autoencoder (Rombach et al., 2022). It uses the diffusion model to learn the data distribution in hidden space, and generate images by sampling a hidden vector and project it back to the image space. This model requires large dataset for pre-training and is commonly used for fine-tuning scenarios because of the good performance in pre-trained model and fast training speed of fine-tuning.

Generalization to fine-tuning GDMs. To use our method and enhance the pattern uniformity in the fine-tuning settings, we make two modifications. 1) In stead of enhancing the uniformity in pixel space, we add and optimize the watermark in hidden space and enhance the uniformity in hidden space. 2) Instead of using PGD to limit the budget, we add l_2 norm as a penalty in our objective.

Experiment details. We use the *pokemon-blip-captions* dataset as the protected images and following the default settings in *huggingface/diffusers/examples/text_to_image* (von Platen et al., 2022) to finetune a Stable Diffusion, which is one of Latent Diffusion Models.

J. Visualization

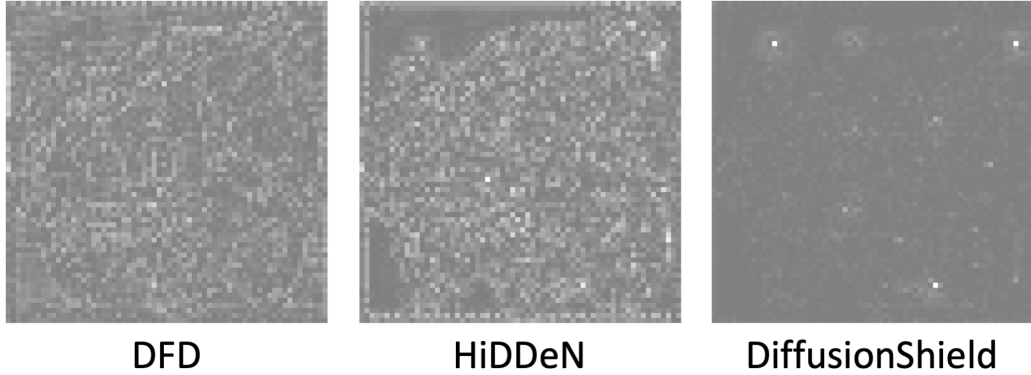


Figure 13. The change of hidden space after watermarking.

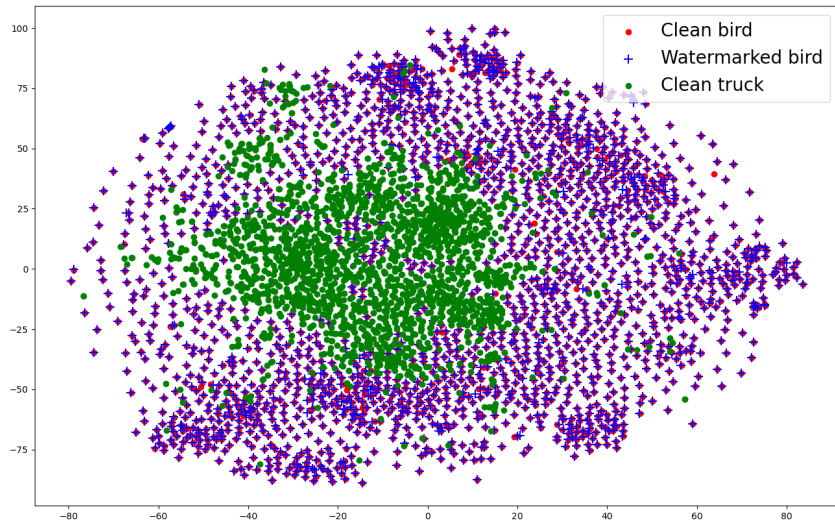


Figure 14. The change of hidden space after watermarking.

Visualization of hidden space of Stable Diffusion. In Figure 13, we visualize the change of hidden space. The hidden space of SD is in shape of $[4, 64, 64]$ which has 4 channels. We visualize one of channel and find that the change of DFD and HiDDeN is much obvious than ours.

Visualization of feature space extracted by Contrastive Learning In Figure 14, we visualize the influence of watermark on the feature space. We use Contrastive Learning (Chen et al., 2020) to extract the feature of both clean and watermarked class.